UNIVERSIDADE BEIRA INTERIOR

Development of multifunctional graphene oxide based nanomaterials for cancer therapy

Bruna Daniela Lopes Melo

Dissertação para obtenção do Grau de Mestre em
Ciências Biomédicas
(2º ciclo de estudos)

Orientador: Doutor Duarte Miguel de Melo Diogo
Co-orientador: Prof. Doutor Ilídio Joaquim Sobreira Correia
Co-orientador: Mestre Ana Rita Lima Sousa

setembro de 2020

“O valor das coisas não está no tempo que elas duram, mas na intensidade com que acontecem. Por isso existem momentos inesquecíveis, coisas inexplicáveis e pessoas incomparáveis.” - Fernando Pessoa

Dedication

Dedico este trabalho à minha família, especialmente aos meus pais, à minha irmã e aos meus avós, por todo o apoio, força e encorajamento que me deram ao longo de todo o meu percurso académico.

Acknowledgments

Primeiro, quero agradecer ao meu co-orientador, Professor Doutor Ilídio Correia, pela oportunidade que me deu, por me ter deixado integrar este grupo de investigação e por me ter proporcionado todas as condições para que eu pudesse desenvolver este trabalho. Agradeço-lhe também por toda a ajuda, todos os ensinamentos e toda a exigência, que me fizeram crescer tanto a nível profissional como pessoal.

Ao meu orientador, Doutor Duarte Diogo, estou profundamente grata por toda a ajuda, pela paciência e por todo o tempo que despendeu comigo ao longo desta tese. Agradeço-lhe também por todo o conhecimento que me transmitiu, pela sua motivação, por nunca me deixar desistir e por me ajudar sempre a encontrar uma alternativa nos momentos em que parecia não existir solução. Sem o seu apoio e orientação este trabalho não teria sido possível.

À minha co-orientadora Mestre Rita Sousa, estou imensamente grata por toda a sua ajuda, por todos os conhecimentos que me transmitiu, por todo o tempo despendido, por toda a sua dedicação, pela enorme paciência, pelo esforço e pela compreensão ao longo desta tese.

Às restantes "Frozens", Cátia, Carolina e Sol, agradeço por estarem sempre dispostas a ajudar e pelos momentos partilhados.

Às minhas "Marias": Inês, Rafa e Mariana, obrigado por toda a vossa paciência, pela ajuda, pela companhia, pelo incentivo, pelas brincadeiras, pelas idas ao MC, pelas boleias e sobretudo pela amizade.

Aos restantes colegas de laboratório transmito um obrigado por toda a ajuda, apoio, brincadeiras e por todos os momentos partilhados.

À Catarina, por ser a minha maior amiga, que me atura desde a infância e mesmo longe, esteve sempre presente. À Mónica por ser a irmã que a Covilhã me deu e por me aturar desde o primeiro ano da licenciatura.

Por fim, quero agradecer à minha família. Agradeço aos meus pais por acreditarem em mim, por serem o meu suporte e a minha força, e por todas as chamadas diárias, que por mais curtinhas que fossem, nunca falharam. À minha mãe por acreditar em mim e me dar sempre uma palavra de carinho e motivação. Ao meu pai, por ser a pessoa mais

alegre que conheço, por me fazer rir sempre e por me incentivar a querer chegar mais longe. À minha irmã, que mesmo já crescida, será sempre a minha pequenina que está sempre pronta para me “chatear” mas também para me dar palavras carinhosas. Aos meus avós, que já partiram, mas que caminham sempre comigo.

Por fim, agradeço também a Deus.

Resumo

O cancro da mama é uma das doenças com maior taxa de mortalidade associada. Este facto está relacionado com a baixa eficácia das terapias, como por exemplo a radio e a quimioterapia, usadas em meio clínico.

Para ultrapassar esta baixa eficácia e os efeitos secundários associados, os investigadores têm procurado desenvolver novas abordagens para o tratamento do cancro da mama. Recentemente, a Terapia Fototérmica (do inglês *Photothermal Therapy* (PTT)) mediada por nanomateriais tem apresentado resultados bastante promissores. Nesta modalidade terapêutica, os nanomateriais, devido às suas características físico-químicas, conseguem acumular-se no tumor. Posteriormente, a zona tumoral é irradiada com luz com comprimento de onda na região do infravermelho próximo (do inglês *Near Infrared* (NIR)). A interação da luz NIR com os nanomateriais acumulados no tumor induz um aumento de temperatura local (hipertermia), que pode causar a morte das células cancerígenas.

De entre os vários nanomateriais que têm sido estudados para aplicação na PTT do cancro, o Óxido de Grafeno (do inglês *Graphene Oxide* (GO)) tem sido amplamente explorado devido à sua absorção no NIR. Após interação com esta radiação, o GO produz um aumento de temperatura que pode causar danos celulares. Para além disto, este nanomaterial tem uma matriz aromática que lhe permite encapsular uma grande variedade de compostos, exibindo, portanto, uma grande versatilidade. No entanto, a aplicação direta do GO na PTT do cancro é limitada por dois fatores: i) a baixa estabilidade coloidal do GO, o que faz com que precipite em fluidos biológicos, e ii) a fraca capacidade fototérmica do GO, o que conduz à administração de doses elevadas/uso de radiação intensa para alcançar um efeito terapêutico adequado.

No trabalho de investigação que desenvolvi durante o meu mestrado, o GO foi funcionalizado com um conjugado de Metacrilato de Sulfobetaína-Albumina de Soro Bovino (SBMA-*g*-BSA) e o IR780 foi encapsulado na sua estrutura, com o intuito de melhorar a sua estabilidade coloidal e capacidade fototérmica, respetivamente. Os resultados obtidos mostraram que o GO funcionalizado com SBMA-*g*-BSA (SBMA-BSA/GO) apresenta uma distribuição de tamanhos e citocompatibilidade adequadas para a sua aplicação na terapia do cancro. Quando o SBMA-BSA/GO foi colocado em contacto com meio com relevância biológica, o seu tamanho apenas aumentou em 5 % durante 48 h. Por outro lado, o GO revestido apenas com BSA (sem

funcionalização de SBMA) teve um acréscimo de 31 % no seu tamanho neste período. Ao encapsular o IR780 na estrutura grafítica do GO, a absorção deste nanomaterial na zona do NIR aumentou em cerca de 5,6 vezes, o que permitiu duplicar a sua capacidade fototérmica. Nos estudos realizados *in vitro*, a viabilidade das células do cancro da mama não foi afetada pela sua incubação com SBMA-BSA/GO juntamente com radiação NIR. Por outro lado, a combinação de IR/SBMA-BSA/GO com irradiação NIR induziu a morte destas células (viabilidade celular inferior a 2 %). Assim, o IR/SBMA-BSA/GO apresenta estabilidade coloidal e capacidade fototerapêutica melhoradas, sendo um nanohíbrido promissor para a aplicação na PTT do cancro da mama.

Palavras-chave

IR780;Óxido de Grafeno;Revestimentos baseados em proteínas;Revestimentos Zwiteriónicos;Terapia do cancro;Terapia fototérmica

Resumo Alargado

Atualmente, o cancro é uma das doenças com maior taxa de mortalidade associada. O cancro da mama, em particular, é um dos que mais afeta as mulheres. Este facto está relacionado com a baixa eficácia das terapias, como por exemplo a radio e a quimioterapia, usadas em meio clínico.

Para ultrapassar esta baixa eficácia e os efeitos secundários associados, os investigadores e profissionais de saúde têm procurado implementar novas estratégias para a terapia do cancro. Recentemente, a Terapia Fototérmica (do inglês *Photothermal Therapy* (PTT)) mediada por nanomateriais tem apresentado resultados bastante promissores. Esta modalidade terapêutica explora a utilização de nanomateriais que, por possuírem um conjunto específico de características físico-químicas, conseguem acumular-se no microambiente tumoral após administração intravenosa. Posteriormente, a zona tumoral é irradiada com luz com um comprimento de onda específico, que é absorvida pelos nanomateriais, conduzindo a um aumento de temperatura local que pode causar a morte das células cancerígenas. Nesta abordagem terapêutica o uso de luz com comprimento de onda no infravermelho próximo (750-1000 nm; do inglês *Near Infrared* (NIR)) é fundamental uma vez que esta radiação não interage significativamente com componentes biológicos (p. ex.: água, proteínas, melanina) e possui uma elevada capacidade de penetração nos tecidos.

De entre os vários nanomateriais que têm sido estudados para aplicação na PTT do cancro, o Óxido de Grafeno (do inglês *Graphene Oxide* (GO)) tem sido amplamente explorado devido à sua absorção no NIR. Após interação com esta radiação, o GO produz um aumento de temperatura que pode causar danos celulares. Para além disso, este nanomaterial tem uma matriz aromática que lhe permite encapsular uma grande variedade de compostos, exibindo, portanto, uma grande versatilidade. No entanto, a aplicação direta do GO na PTT é limitada por dois fatores: i) a baixa estabilidade coloidal do GO, o que faz com que precipite em fluidos biológicos, e ii) a fraca capacidade fototérmica do GO, o que conduz à administração de doses elevadas/uso de radiação intensa para alcançar um efeito terapêutico adequado.

No trabalho de investigação que desenvolvi durante o meu mestrado, o GO foi funcionalizado com um conjugado de Metacrilato de Sulfobetaína-Albumina de Soro Bovino (do inglês *Sulfobetaine Methacrylate-grafted-Bovine Serum Albumin*

(SBMA-*g*-BSA)), e o IR780 foi encapsulado na sua estrutura, com o intuito de melhorar a sua estabilidade coloidal e capacidade fototérmica, respetivamente.

O SBMA-*g*-BSA foi selecionado para revestir o GO uma vez que os domínios hidrofóbicos da BSA conseguem adsorver-se na superfície aromática do GO. Por outro lado, a funcionalização de nanomateriais com SBMA tem a capacidade de aumentar a estabilidade coloidal dos mesmos, favorecendo o seu tempo de circulação e acumulação no tumor. Após a sua síntese, o polímero anfifílico SBMA-*g*-BSA foi utilizado na funcionalização do GO através de um processo de sonicação (SBMA-BSA/GO). Tirando partido da mesma metodologia, procedeu-se à encapsulação do IR780 no SBMA-BSA/GO (IR/SBMA-BSA/GO).

Os resultados obtidos demostraram que o SBMA-BSA/GO e IR/SBMA-BSA/GO apresentam uma distribuição de tamanhos adequada para a sua aplicação na terapia do cancro. Quando o SBMA-BSA/GO e IR/SBMA-BSA/GO foram colocados em contacto com meio com relevância biológica, os seus tamanhos apenas aumentaram em 8 % durante 48 h. Por outro lado, o GO revestido apenas com BSA (sem funcionalização de SBMA) teve um acréscimo de 31 % no seu tamanho neste período. Ao encapsular o IR780 na estrutura grafítica do SBMA-BSA/GO, a absorção deste nanomaterial na zona NIR aumentou em 5,6 vezes, o que permitiu duplicar a sua capacidade fototérmica. Nos estudos *in vitro*, a viabilidade das células do cancro da mama não foi afetada pela sua incubação com SBMA-BSA/GO juntamente com radiação NIR. Por outro lado, a combinação de IR/SBMA-BSA/GO com irradiação NIR induziu a morte destas células (viabilidade celular inferior a 2 %). Assim, o IR/SBMA-BSA/GO apresenta estabilidade coloidal e capacidade fototerapêutica melhoradas, sendo um nanohíbrido promissor para a aplicação na PTT do cancro da mama.

Abstract

Breast cancer remains as one of the deadliest diseases affecting the worldwide population. The high mortality rate exhibited by this disease can be attributed to the limitations of the treatments currently in use in the clinic (*e.g.* radiotherapy, chemotherapy), which display a low therapeutic efficacy and induce adverse side effects in patients. Therefore, there is an urgent demand for innovative therapeutic approaches that can enhance breast cancer survival rates.

Recently, nanomaterials' mediated Photothermal Therapy (PTT) has been showing promising results for cancer treatment. This therapeutic modality employs nanostructures that, due to their specific set of physicochemical characteristics, can accumulate at the tumor site. Afterwards, this zone is irradiated with Near Infrared (NIR) light and the tumor-homed nanomaterials induce a local temperature increase (hyperthermia) that can induce damage to cancer cells.

Among the several nanomaterials with potential for cancer PTT, Graphene Oxide (GO) has been extensively investigated due to its absorption in the NIR. After interacting with this radiation, GO produces a temperature increase that can cause damage to cancer cells. In addition, this nanomaterial has an aromatic matrix that can be used to encapsulate a wide variety of compounds, thus having a great versatility. However, the direct application of GO in cancer PTT is limited by two factors: i) the low colloidal stability of GO, which causes its precipitation in biological fluids, and ii) the poor photothermal capacity of GO, which leads to the use of high doses/intense radiation in order to achieve an adequate therapeutic effect.

In this MSc research work, GO was functionalized with an albumin based amphiphilic coating containing Sulfobetaine Methacrylate (SBMA) brushes (SBMA-*g*-BSA) and was loaded with IR780, with the intent to improve its colloidal stability and photothermal capacity, respectively. The results revealed that GO functionalized with SBMA-*g*-BSA (SBMA-BSA/GO) presents an adequate size distribution and cytocompatibility for cancer-related applications. When in contact with biologically relevant media, the size of the SBMA-functionalized GO derivatives only increased by 8 % after 48 h. In the same condition and period, the non-SBMA functionalized GO (BSA coated GO) suffered a 31 % increase in its size. By loading IR780 into SBMA-BSA/GO (IR/SBMA-BSA/GO), the nanomaterials' NIR absorption increased by 5.6-fold. In this way, the IR/SBMA-BSA/GO could produce a up to 2-times higher photoinduced heat

than SBMA-BSA/GO. In *in vitro* cell studies, the combination of NIR light with SBMA-BSA/GO did not induce photocytotoxicity on breast cancer cells. In stark contrast, the interaction of IR/SBMA-BSA/GO with NIR light caused the ablation of cancer cells (cell viability < 2 %). Overall, IR/SBMA-BSA/GO displays a greatly improved colloidal stability and phototherapeutic capacity, being a promising hybrid nanomaterial for application in the PTT of breast cancer cells.

Keywords

Cancer therapy, Graphene Oxide, IR780, Photothermal therapy, Protein-based coatings, Zwitterionic coatings.

Index

List of Figures

List of Abbreviations

ABC	Accelerated Blood Clearance
ANOVA	Analysis of Variance
BSA	Bovine Serum Albumin
BSA/GO	BSA functionalized GO
DLS	Dynamic Light Scattering
DMEM-F12	Dulbecco's Modified Eagle's Medium-F12
DTT	DL-Dithiothreitol
ECM	Extracellular Matrix
EPR	Enhanced Permeability and Retention
FBS	Fetal Bovine Serum
FTIR	Fourier Transform Infrared Spectroscopy
GO	Graphene Oxide
IR/SBMA-BSA/GO	IR780 loaded SBMA-BSA/GO
MCF-7	Michigan Cancer Foundation-7
MTS	3-(4,5-dimethylthiazol-2-yl)-5-(3-carboxymethoxyphenyl)-2-(4-sulfophenyl)-2H-tetrazolium
NHDF	Normal Human Dermal Fibroblasts
NIR	Near Infrared
ns	Non-significant
PEG	Poly(ethylene glycol)
PTT	Photothermal Therapy
SBMA	[2-(methacryloyloxy)ethyl]dimethyl-(3-sulfopropyl)ammonium hydroxide
SBMA-*g*-BSA	BSA grafted with SBMA
SBMA-BSA/GO	SBMA-*g*-BSA functionalized GO
S.D.	Standard Deviation
UV-Vis-NIR	Ultraviolet-Visible-Near Infrared
TEM	Transmission Electron Microscopy

Chapter 1

Introduction

1. Introduction

1.1. Cancer development, hallmarks, and treatments

Cancer is one of the main diseases affecting the human population and it is a leading cause of death in the world. According to the latest report of the American Cancer Society, 1 806 590 new cases of cancer will be diagnosed only in the USA during 2020 [1]. Moreover, it is estimated that 606 520 patients will die from cancer in the USA, only in 2020 [1].

Cancer is characterized by an abnormal and uncontrolled growth of cells caused by multiple genetic and epigenetic changes, leading to a dysregulated balance of proliferation and death, that ultimately evolves into a population of diseased cells that can invade tissues and metastasize to distant sites within the human body [2]. During the long process of tumor development and malignant progression, cancer cells acquired new characteristics designated by hallmarks of cancer (Figure 1) [3]. The distinct hallmarks consist of cancer cells' ability to: 1) sustain a proliferative signaling pathway; 2) evade growth suppressors; 3) avoid destruction by the immune system; 4) have replicative immortality; 5) activate the invasion and metastasis process; 6) induce angiogenesis; 7) resist to cell death; and 8) deregulate cellular energetics and metabolism [3, 4].

Cancer cells can synthesize stimulatory growth factors (autocrine signaling), which makes them less dependent on their environment to proliferate [4]. Furthermore, cancer cells can also interact with the stroma cells (*e.g.* cancer-associated fibroblast, endothelial cells) and stimulate them to produce growth factors that will promote cancer cells' proliferation [4, 5]. Cancer cells have an increased expression of growth factors' receptors, which are in a constant active state, further sustaining their growth [4, 6]. Additionally, these cells can maintain their proliferative activity by down-regulating the expression of tumor suppressor genes (*e.g.* tumor suppressor p53 and retinoblastoma associated protein) [3, 4].

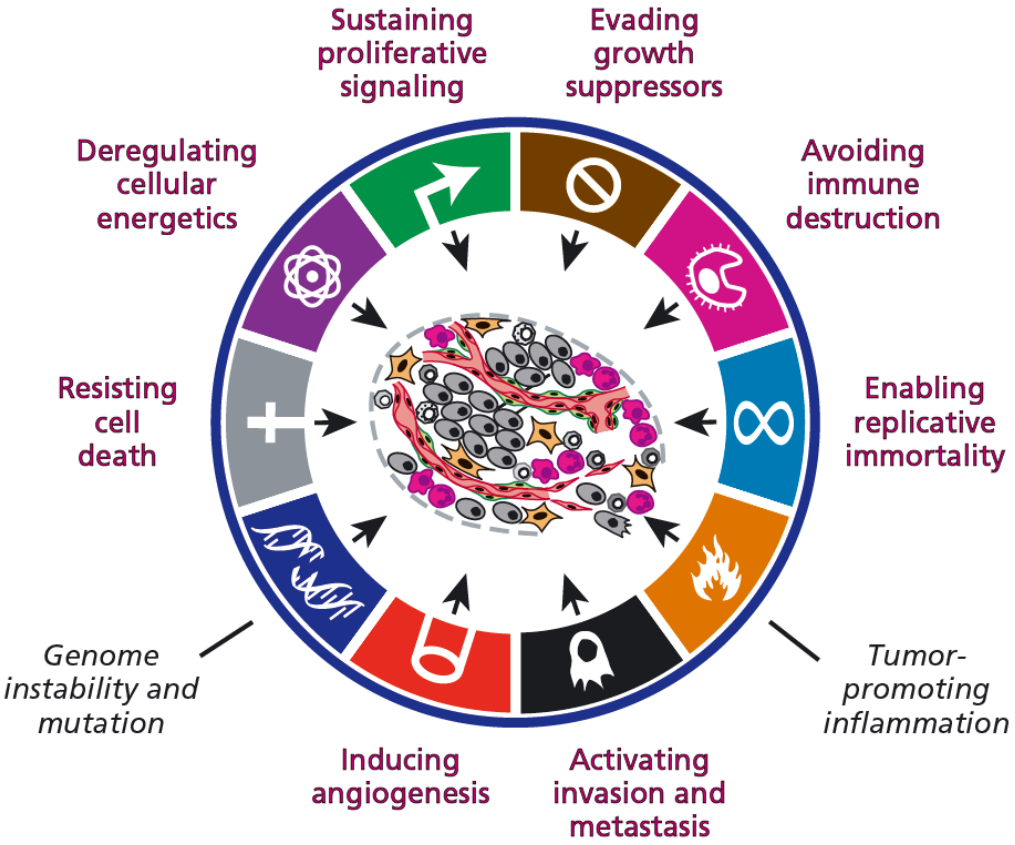

Figure 1: The cancer hallmarks described by Hannah and Weinberg. Initially, only six hallmarks were proposed, which consist of cancer cells' capacity to i) maintain a proliferative signaling, ii) evade growth suppressors, iii) have unlimited replicative activity, iv) invade other tissues, v) prompt angiogenesis, and vi) resist cell death mechanisms. In 2011, two new hallmarks were proposed, namely the cancer cells' capacity to i) evade destruction by the immune system, and ii) deregulate cellular metabolism (Adapted from [3]).

Additionally, cancer cells overexpress telomerase, which is responsible for constantly adding nucleotide repeats to the end of the chromosomes after cell division, ultimately avoiding the degradation of telomeres and their end-to-end fusion [3, 4]. This feature confers a replicative immortality to cancer cells, as it protects them from senescence and apoptosis.

Furthermore, cancer cells have a high metabolic activity, permanently demanding nutrients and a well-established gas exchange [3, 4]. Thus, for a sustained growth, tumors require an extensive blood vessel system, which is ensured by angiogenesis [3]. The newly formed 3D vasculature is disorganized, with considerable fenestrations that support cancer cells' leakage into other sites, where they can form micrometastasis that can evolve into larger tumors [4]. This complex invasion-metastasis cascade is mediated by the downregulation of the expression of adhesion molecules (*e.g.* E-cadherin) and enhanced expression of mesenchymal markers associated with cell migration (*e.g.* N-cadherin) [7]. Furthermore, tumor-infiltrating bone

marrow-derived cells, such as macrophages, can also supply matrix-degrading enzymes to the tumor microenvironment, facilitating the metastatic process [4, 8].

Additionally, cancer cells have the ability to evade the programmed cell death (apoptosis), mainly by mutations in the tumor suppressor gene p53, overexpression of anti-apoptotic factors (*e.g.* Bcl-2, Bcl-xL, and Bcl-w) or down-regulation of pro-apoptotic factors (*e.g.* Bax or Bim) [3, 4].

More recently, two new emerging cancer hallmarks were identified and added to the original list: the cancer cells' capacity to deregulate cellular energetics and to avoid immune destruction [3]. The tumor mass presents an hypoxic region, and cancer cells within this region have an upregulated expression of HIF-1α (a transcription factor responsible to regulate the cells' metabolism) [9, 10]. In this way, cancer cells can convert pyruvate into lactate to obtain the energy necessary to evolve in an uncontrolled manner (the Warburg effect), resulting in the acidification of the tumor microenvironment [11, 12]. This metabolic change is also associated with the presence of oncogenes (*e.g.* RAS and MYC) and the absence of tumor suppressor genes (*e.g.* p53) [3]. Additionally, the immune system is a key participant in the control of cancer progression. However, cancer cells develop several mechanisms that help them evade the detection/elimination by the immune system cells [13, 14]. For example, cancer cells express the Programmed Death Ligand 1 (PD-L1). This ligand binds to its receptor (PD-1), expressed in several cells of the immune system, culminating in the suppression of antitumoral T cell responses [15, 16].

The acquisition of these hallmarks is facilitated by the genome instability and mutations that allow an increasing sensitivity towards mutagenic agents or a capacity to circumvent the cellular DNA repair machinery [3, 4]. Furthermore, tumor-associated inflammation can also contribute to assist cells in advancing to a malignant state [3, 4].

1.2. Breast cancer

Breast cancer is a malignant neoplasm originating from breast tissue, most commonly from the inner lining of milk ducts or the lobules that supply the ducts with milk [17]. This type of cancer affects women all over the world. Just in the USA, approximately 48 530 new cases of breast ductal carcinoma are expected to be diagnosed in women during 2020 [1]. In the case of Portugal, approximately 6 000 new cases of breast cancer are detected annually, and about 1 500 women die from this disease [18]. The

risk of developing breast cancer increases with the age, being generally diagnosed after the 55 years-old mark [17, 19]. Genetic mutations (*e.g.* in BRCA1 and BRCA2) increase the probability of developing breast cancer [17]. The reproductive history, early menstrual periods, age of menopause and family history also increase the likelihood of developing this disease [17, 19]. Other risk factors that strongly affect the progress of breast cancer are lifestyle related (*e.g.* physical inactivity, excessive weight, alcohol consumption) [17, 19].

The normal mammary duct consists of a luminal epithelial cell layer surrounded by myoepithelial cells, which bind to the basement membrane [20, 21]. The healthy breast tissue is also composed of extracellular matrix (ECM) components and several types of stromal cells, including fibroblasts, endothelial and immune system cells (Figure 2) [22].

Different components of the breast tissue (*e.g.* macrophages, myoepithelial and endothelial cells, and ECM molecules) play a critical role in the morphogenesis of the mammary duct [21-23]. The stroma cells maintain epithelial polarity and inhibit uncontrolled cell growth and neoplastic transformation [21, 22]. Myoepithelial cells have been recognized as natural suppressors of breast tumors, since they produce the basement membrane and represent a physical barrier around the epithelial cells [21, 22].

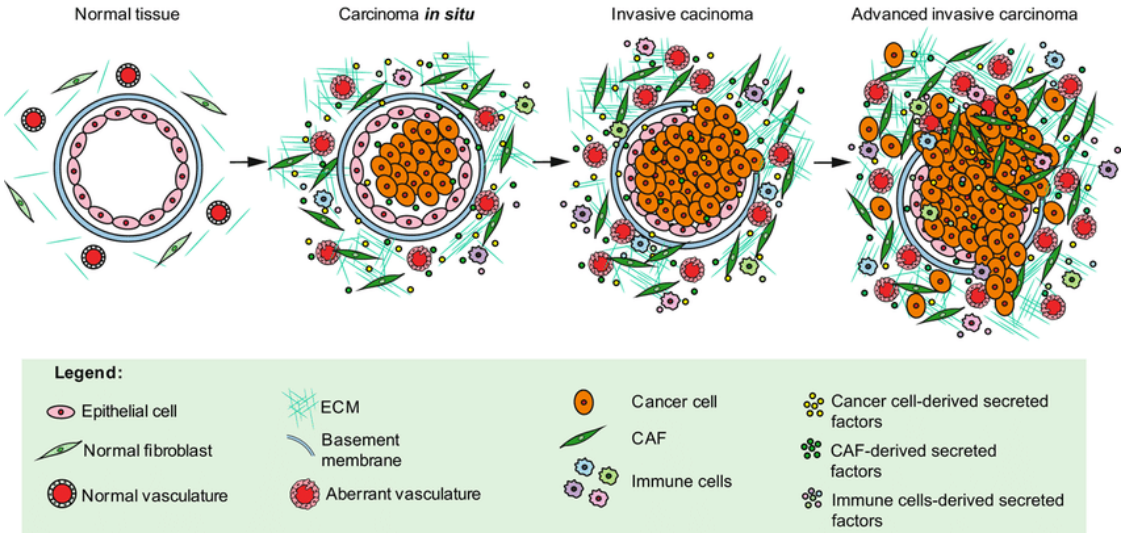

Figure 2: Schematic representation of the breast cancer progression and development. The epithelial cells that are present in the ducts endure several changes, leading to an increase in infiltrating cells (*e.g.* stromal cells and leukocytes) and decrease in the number of myoepithelial cells, culminating in the degradation of the basement membrane and in the formation of an *in situ* carcinoma. When the myoepithelial cells are completely absent, the carcinoma changes into an invasive state (Adapted from [22]).

Breast tumorigenesis evolves via a sequential progression through defined stages, beginning with epithelial cells' hyperproliferation and progressing to *in situ*, invasive and metastatic carcinomas [17, 23]. This process initiates with the acquisition of genetic and epigenetic changes in all types of cells present in the breast duct. These changes ultimately lead to a decrease in the number of myoepithelial cells, to an early degradation of the basement membrane, and to an increase in the stromal population [23], culminating in an *in situ* carcinoma (Figure 2). In the progression of breast cancer, the transition from *in situ* to invasive carcinoma occurs with the loss of the myoepithelial cell layer and the basement membrane (Figure 2) [22]. Subsequently, the breast cancer cells can invade other tissues, originating metastases [22].

Additionally, cancer-associated fibroblast interact with cancer cells through paracrine signaling, creating a microenvironment that influences their proliferation [24]. On the other hand, tumor-associated macrophages are recruited to the tumor microenvironment, secreting cytokines and growth factors that contribute to the angiogenesis and invasion processes [23, 24].

According to the stage of breast cancer development, its treatment includes the surgical resection of the tumor (for early stage), or radiotherapy and chemotherapy (mainly for late stage) [25]. These two last therapies are characterized by requiring high doses and by presenting a low selectivity, causing notorious side effects [25]. Additionally, cancer cells tend to develop resistance to chemo and radiotherapy, which further decreases the treatments' efficacy [24, 26].

In order to overcome these limitations, researchers have been focused on investigating the potential of nanomaterials' mediated Photothermal Therapy (PTT) due to its capacity to induce the thermal ablation of cancer cells with minimal systemic exposure [27, 28].

1.3. Nanomaterials mediated photothermal therapy

The use of nanomaterials for cancer PTT has been a topic of intense pre-clinical investigation in the last decade [29]. These nanostructures, due to their specific set of physicochemical properties, can reach the tumor site when administered intravenously (Figure 3) [27, 30, 31]. To accumulate at the tumor site, nanomaterials can extravasate through the tumor's leaky vasculature, which presents large fenestrations (200-1200 nm) [27]. Furthermore, the lymphatic drainage is compromised in the

tumor area, which promotes the retention of the nanomaterials in the tumor microenvironment [31-33]. This phenomenon is known as the Enhanced Permeability and Retention (EPR) effect [31, 33]. Besides achieving tumor accumulation by using the EPR effect, nanomaterials can also accumulate in the tumor zone by extravasating through the dynamic vents (also called eruptions) that spontaneously occur in the tumor's vasculature [34]. Once at the tumor site, nanomaterials must penetrate into the tumor mass for subsequently achieving internalization in the cancer cells.

Afterwards, the tumor site is externally irradiated with Near Infrared (NIR; 750-1000 nm) light and the tumor-homed nanoparticles absorb this radiation, converting it into heat that can cause damage to cancer cells (Figure 3) [27]. In general, a hyperthermia up to 41-45 °C originates sublethal and reversible damages on cells (*e.g.* alterations in the metabolic functions, inhibition of the DNA repair mechanisms, or sensibilization to other therapies) [27, 35]. Furthermore, the attained temperature increase can augment the blood circulation in the tumor zone, allowing the accumulation of a greater number of nanoparticles at this site [27]. On the other hand, a nanomaterials' mediated photoinduced heat to 50 °C (or above) can cause the collapse of the cancer cells' membrane, the denaturation of proteins and disfunction in the enzymatic and mitochondrial activities, ultimately leading to cancer cells death by necrosis [27, 35].

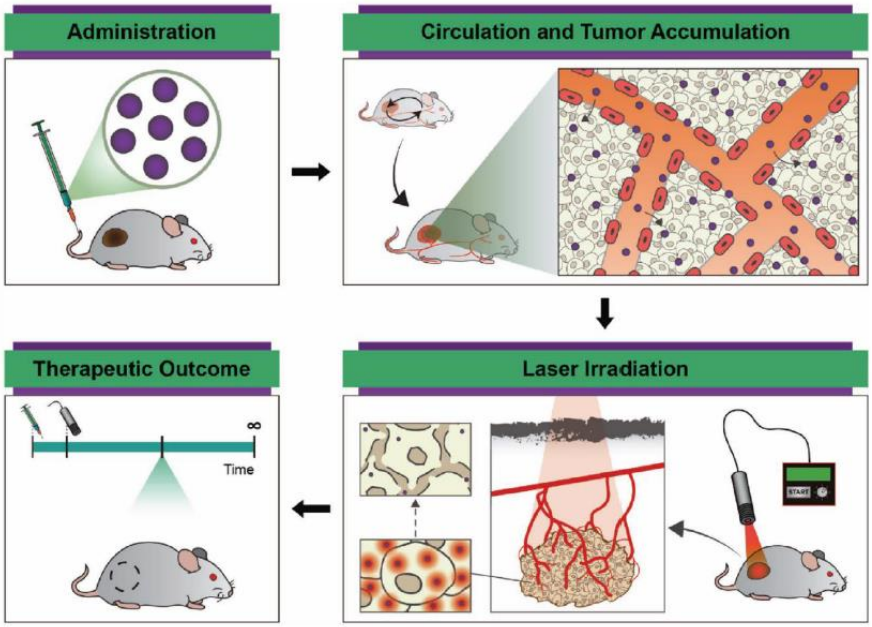

Figure 3: Representation of the events occurring in PTT mediated by nanomaterials. Firstly, the NIR-responsive nanomaterials are administered intravenously and, due to their physicochemical characteristics, they become accumulated in the tumor microenvironment. Afterwards, this zone is irradiated with NIR laser light. The nanomaterials absorb the NIR light energy and release it as heat. If the temperature increase attained is sufficiently high, complete tumor eradication can be achieved (Adapted from [27]).

In this therapeutic approach, the use of NIR light is crucial since the majority of the biological components (*e.g.* water, proteins, melanin) have a minimal/irrelevant NIR light absorption (Figure 4) [27]. Such grants NIR light a deep tissue penetration and minimal off-target heating [28]. In this way, nanomaterials' mediated PTT can produce a spatio-temporal controlled therapeutic effect.

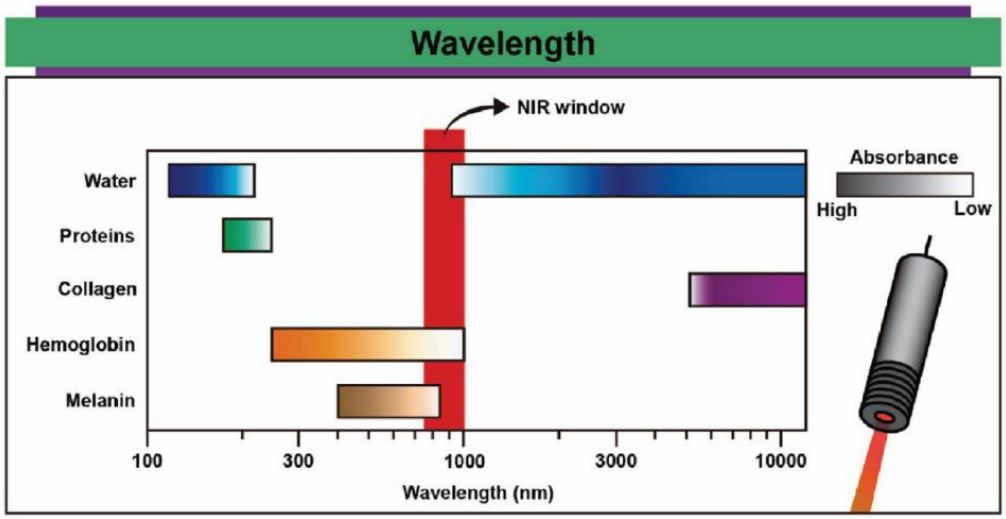

Figure 4: Schematic representation of the biological transparency window. Most of the biological components display minimal absorption in the NIR region (between 750 and 1000 nm, represented as a vertical red bar). In this way, using NIR light in PTT is of utmost importance, since it ensures a high penetration depth and low off-target interactions (Adapted from [27]).

Therefore, the success of nanomaterials' mediated PTT is influenced by their physicochemical and optical properties [27, 29]. The nanostructures' physicochemical features influence their ability to reach the tumor site, while their optical characteristics dictate mostly the attained photothermal effect [27, 29].

In order to achieve a high tumor uptake, nanomaterials should avoid rapid renal clearance (common for nanomaterials with a size inferior to 5 nm) and uptake by the liver (common for nanomaterials with a size inferior to 50 nm) and spleen (common for nanomaterials with a size superior to 200 nm) [32]. Taking these and the EPR size constrains into account, nanomaterials should have a size between 50 and 200 nm in order to achieve a high tumor uptake with minimal accumulation in the liver/spleen [27].

The nanoparticles' surface charge is another important characteristic that influences their blood circulation time, tumor penetration, and cellular internalization [31, 32]. Nanostructures with a highly positive or negative surface charges display i) a greater

opsonization during blood circulation; ii) an augmented interaction with reticuloendothelial system cells or erythrocytes; and iii) an enhanced interaction with the tumor's ECM components [32]. These interactions decrease the likelihood of the nanoparticles to reach the tumor site and become internalized by cancer cells. In this way, nanomaterials that present a neutral surface charge (zeta potential between -10 and +10 mV) are considered ideal [27, 31].

The nanomaterials' corona composition is also crucial for their biological fate. Usually, the nanomaterials surface is decorated with different hydrophilic components, such as poly(ethylene glycol) (PEG) [36, 37], poly(2-oxazolines) [38, 39] or zwitterionic polymers [40, 41], that prevent the opsonization of the nanoparticles by blood circulating proteins, thus increasing their blood circulation time and tumor accumulation [36, 42, 43]. Additionally, the nanoparticles' surface can also be functionalized with components that grant them targeting capacity (*e.g.* folic acid or anti-CD44 antibodies) [44, 45]. These components can bind to specific receptors that are overexpressed in cancer cells' membrane, and thus improve the nanoparticles' selectivity towards the cancer cells [46].

The nanomaterials' optical properties are also important to achieve an appropriate therapeutic outcome. In general, nanomaterials aimed for application in cancer PTT should have a high NIR absorption in order to interact with the NIR light [27, 47]. Furthermore, these should also present a high photothermal conversion efficiency [27, 47]. In this regard, inorganic nanostructures (*e.g.* gold nanorods [48, 49], graphene derivatives [50, 51]) with a high NIR absorption have been the ones mostly explored for cancer PTT [27]. When compared to their organic equivalents (*e.g.* nanostructures encapsulating NIR absorbing small molecules such as indocyanine green [52, 53] or IR808 [54, 55]), the NIR-responsive inorganic nanomaterials present a higher photothermal conversion efficiency and photostability [28]. Recently, graphene oxide (GO) and its derivatives, due to their high NIR absorption, good physicochemical and optical properties, have emerged for application in cancer PTT [56-58].

1.4. Graphene Oxide in cancer photothermal therapy

GO is a 2D material composed of a graphitic lattice decorated with different oxygen functional groups (*e.g.* hydroxyl, carboxyl, and epoxide groups), that has been extensively investigated for cancer PTT (Figure 5) [59, 60]. This material is usually

obtained from graphite through oxidation and exfoliation processes (*e.g.* using the improved Hummers' method) [61]. Subsequently, the obtained material is subjected to multiple sonication steps in order to attain nanosized GO [62]. In this way, the synthesis of GO is a relatively simple process when compared to the production and purification steps required to attain other types of inorganic nanomaterials with NIR absorption (*e.g.* carbon nanotubes [63], gold nanorods [64]).

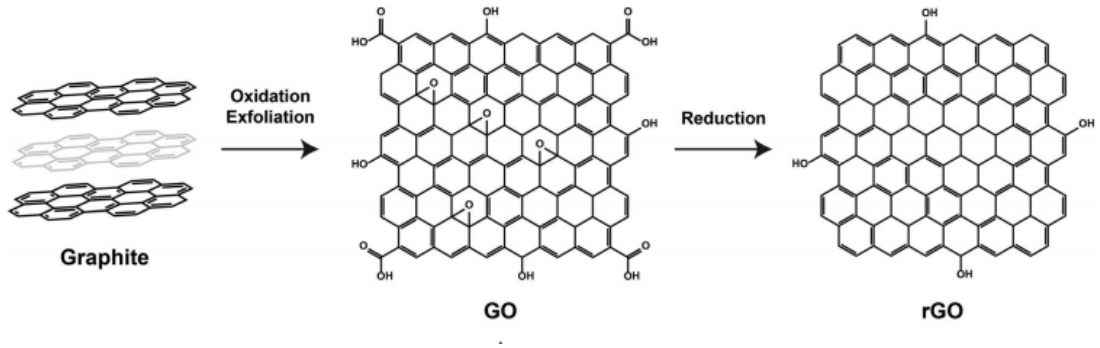

Figure 5: Schematic representation of the synthesis of GO and the reduction of GO (Adapted from [65]).

GO displays a broad absorption in the NIR range, enabling its application in cancer PTT [66]. For instance, Luo *et al.* verified that GO-based materials could produce a temperature increase of about 32 °C upon irradiation (808 nm, 2 W/cm^2, 5 min; 30 μg/mL), which led to a decrease of cancer cells' viability to 75 % [55]. Furthermore, the aromatic lattice of GO displays a high surface area capable of adsorbing a wide variety of compounds (*e.g.* chemotherapeutic drugs, proteins) through π–π stacking and hydrophobic interactions [66, 67].

Despite GO's potential, this nanomaterial presents a low colloidal stability, hence precipitating in biological fluids [58, 66, 68]. To address this limitation, before *in vivo* applications, GO is generally functionalized with PEG (a hydrophilic polymer with a good biocompatibility) [56, 69]. The coating of nanomaterials with PEG confers colloidal stability and protects them from interaction with blood components, thereby prolonging their blood circulation time [37, 70, 71]. For example, Yang *et al.* verified that PEGylated GO derivatives display a long blood circulation time ($t_{1/2}$ = 1.5 h), thereby achieving a high tumor uptake [72].

Despite the benefits of PEGylation, recently it was unveiled that PEG coated GO derivatives suffer from the so-called Accelerated Blood Clearance (ABC) phenomenon [73]. In brief, the intravenous administration of PEG coated nanomaterials induces the production of anti-PEG antibodies, which will prompt the

rapid clearance of these nanomaterials from circulation in subsequent injections [74, 75]. In this way, it is of utmost importance to discover novel materials to functionalize GO that can improve GO colloidal stability and blood circulation time, and that, at the same time, do not trigger the ABC phenomenon.

On the other hand, GO presents a modest photothermal capacity, thus requiring the use of high doses or intense radiation for *in vivo* cancer PTT [65]. For example, Yin *et al.* verified that the PTT mediated by Hyaluronic Acid-functionalized GO only induces a reduction of the tumor's growth, even using a highly intense radiation (808 nm, 5 W/cm^2, 10 min) [76]. To circumvent this limitation, GO has been reduced using hydrazine hydrate [77, 78]. This chemical reduction restores the nanomaterials' graphitic lattice, hence improving their NIR absorption [50, 77]. For instance, Robinson and co-workers demonstrated that hydrazine hydrate reduced GO has an up to 6.8-times higher NIR absorption than GO [79]. Due to this property, the hydrazine hydrate reduced GO originated a photoinduced heat 2.3-times greater than that originated by GO [79].

However, the reduced GO attained using hydrazine hydrate lacks water solubility and is not biocompatible [78-81]. Alternatively, researchers have been incorporating other NIR-responsive nanomaterials (*e.g.* gold nanorods [82]) on the surface of GO in order to increase its photothermal capacity. For example, Xu *et al.* produced a gold nanorod-GO hybrid that, when irradiated with NIR light (808 nm, 4 W/cm^2, 8 min), induced a 4-times higher temperature variation than GO (40 *vs.* 10 °C, respectively) [83]. However, the production of these nanohybrids is a complex and laborious process. Thereby, it is fundamental to develop new approaches to enhance the photothermal capacity of GO.

1.5. Engineering Graphene Oxide nanomaterials with an enhanced colloidal stability and photothermal capacity

Addressing the poor colloidal stability of GO as well as its subpar photothermal capacity is crucial to enhance the potential of this nanomaterial for cancer PTT.

To address the poor colloidal stability of GO, its functionalization with 2-(methacryloyloxy) ethyl] dimethyl-(3-sulfopropyl) ammonium hydroxide (SBMA)-containing materials appears to be a promising approach. SBMA-based

polymers are known to possess excellent antifouling properties [84-87], thus preventing protein adsorption [43]. Alves *et al.* recently demonstrated that the coating of protein based nanoparticles with SBMA increases their stability in biologically relevant media [88]. The functionalization of nanomaterials with SBMA-based polymers can also improve the nanostructures' blood circulation time, leading to a high tumor uptake [89]. As importantly, the ABC phenomenon has not been reported for SBMA-coated nanoparticles [90]. In this regard, Men *et al.* demonstrated that the blood circulation time of SBMA-coated nanomaterials in the first and second intravenous injections is equivalent [90].

On the other hand, the photothermal capacity of GO could be enhanced by incorporating IR780 in its aromatic lattice. IR780 is a hydrophobic small molecule that presents a high NIR absorption [91, 92]. As importantly, the photothermal potential of IR780 is superior or comparable to that displayed by other NIR absorbing small molecules (*e.g.* indocyanine green) [93].

In order to attain a SBMA-containing amphiphilic polymer for GO functionalization, the grafting of SBMA into Bovine Serum Albumin (SBMA-*g*-BSA) can be performed. For this purpose, the primary amine and thiol groups of BSA can be conjugated with SBMA through a Michael addition [88]. Additionally, the hydrophobic segments of BSA can adsorb on the aromatic lattice of GO through hydrophobic-hydrophobic interaction [94]. By taking advantage of this type of interaction as well as from π-π stacking, the IR780 can also be incorporated on the functionalized GO.

Aims

The aim of this MSc Work plan was to produce GO nanomaterials functionalized with SBMA-*g*-BSA encapsulating IR780, with an improved colloidal stability and photothermal capacity, to be applied in breast cancer therapy.

The specific aims of this dissertation are:

- Preparation of SBMA-*g*-BSA functionalized GO (SBMA-BSA/GO);
- Loading of IR780 into SBMA-BSA/GO (IR/SBMA-BSA/GO);
- Characterization of the physicochemical and optical properties of the produced nanomaterials;
- Evaluation of the nanomaterials' colloidal stability and photothermal capacity;
- Evaluation of the cytocompatibility of the SBMA-BSA/GO;
- Evaluation of the phototherapeutic effect mediated by SBMA-BSA/GO and IR/SBMA-BSA/GO towards breast cancer cells.

Chapter 2

Experimental Section

2. Experimental Section

2.1. Materials

Dulbecco's Modified Eagle's Medium F12 (DMEM-F12), IR780, Phosphate Buffered Saline (PBS), DL-Dithiothreitol (DTT), and SBMA were purchased from Sigma–Aldrich (Sintra, Portugal). Methanol was obtained from Honeywell (Oeiras, Portugal). BSA was obtained from Amresco (Pennsylvania, EUA). 3-(4,5-dimethylthiazol-2-yl)-5-(3-carboxymethoxyphenyl)-2-(4-sulfophenyl)-2H-tetrazolium (MTS) was bought from Promega (Madison, WI, USA). Michigan Cancer Foundation-7 (MCF-7) cell line was acquired from ATCC (Middlesex, UK). Normal Human Dermal Fibroblasts (NHDF) were obtained from PromoCell (Heidelberg, Germany). Fetal Bovine Serum (FBS) was bought from Biochrom AG (Berlin, Germany). Cell culture plates and T-flasks were purchased from Thermo Fisher Scientific (Porto, Portugal). GO was provided by NanoPoz (Umultowska Poznan, Wielkopolska). SBMA-*g*-BSA was synthesized as described by Alves *et al.* [88]. Water used in all assays was double deionized (0.22 μm filtered; 18.2 MΩ cm).

2.2. Methods

2.2.1. Production of SBMA-BSA/GO and IR/SBMA-BSA/GO

IR780 loaded SBMA-*g*-BSA functionalized GO (IR/SBMA-BSA/GO) was produced by adapting protocols previously described [38, 88]. Initially, SBMA-*g*-BSA (0.09 mg/mL; 1 mL) and DTT (0.005 mg/mL, 1 mL) were allowed to react for 20 min under constant stirring [88]. Then, GO (200 μg/mL; 0.5 mL) was mixed with the polymer-DTT solution (0.5 mL) and sonicated for 60 min (Branson 5800, Branson Ultrasonics, CT, USA). Then, IR780 (20 μg in methanol) was added to the previous solution, followed by another 30 min of sonication. Subsequently, this solution was dialyzed against water (500–1000 Da cut-off dialysis membrane) for 90 min to remove DTT, methanol and non-loaded IR780. Finally, the recovered solution was centrifuged to remove any aggregates, yielding IR/SBMA-BSA/GO. To produce SBMA-BSA/GO, the process was the same but without the IR780 addition step. As control, GO functionalized with BSA (BSA/GO) was also produced as described above using BSA instead of SBMA-*g*-BSA.

2.2.2. Characterization of SBMA-*g*-BSA, SBMA-BSA/GO and IR/SBMA-BSA/GO

The successful synthesis of SBMA-*g*-BSA was confirmed by Fourier Transform Infrared Spectroscopy (FTIR) using a Nicolet iS10 spectrometer (Thermo Scientific Inc., MA, USA). SBMA-BSA/GO and IR/SBMA-BSA/GO size distribution and zeta potential were evaluated in a Zetasizer Nano ZS (Malvern Instruments Ltd., Worcestershire, UK). The variation of IR/SBMA-BSA/GO, SBMA-BSA/GO and BSA/GO size overtime when dispersed in cell culture medium (DMEM-F12 with 10 % (v/v) of FBS) was also investigated [88]. The nanosized dimensions of SBMA-BSA/GO were confirmed by Transmission Electron Microscopy (TEM, HT7700, Hitachi, Japan; operated at an accelerating voltage of 100 kV). Prior to this analysis, the sample was stained with phosphotungstic acid (2 % (w/v)). UV-Vis-NIR absorption spectroscopy (Evolution 201 spectrophotometer, Thermo Scientific Inc.) was employed to confirm the NIR absorption of SBMA-BSA/GO and IR/SBMA-BSA/GO and the IR780 encapsulation efficiency. Initially, the absorption of IR/SBMA-BSA/GO at 890 nm, when dispersed in water, was analyzed. Then, a standard curve of GO (in water) at 890 nm was used to determine the concentration of GO in the sample (please note that IR780 and SBMA-*g*-BSA do not have absorption at this wavelength). Subsequently, the absorption of IR/SBMA-BSA/GO at 808 nm, when dispersed in water/methanol (1:1 (v/v)), was acquired. Then, the determined concentration of GO and a standard curve of GO at 808 nm (in 1:1 (v/v) water/methanol) was used to determine the absorption of GO at 808 nm. Finally, the absorption of GO (at 808 nm) was subtracted to that of IR/SBMA-BSA/GO (at 808 nm), yielding the IR780 absorption (please note that SBMA-*g*-BSA does not absorb at this wavelength). Finally, a standard curve of IR780 at 808 nm (in 1:1 (v/v) water/methanol) was used to determine the concentration of IR780 in the IR/SBMA-BSA/GO sample [38, 88].

The photothermal capacity of SBMA-BSA/GO and IR/SBMA-BSA/GO was determined by monitoring the temperature variations, using a thermocouple thermometer, upon irradiation of the nanostructures with NIR laser light over a period of 10 min (808 nm, 1.7 W/cm^2) [95].

2.2.3. Evaluation of the cytocompatibility of SBMA-BSA/GO

The cytocompatibility of SBMA-BSA/GO towards MCF-7 cells and NHDF was evaluated through a MTS assay [96]. All cell lines were cultured in DMEM-F12 supplemented with 10 % (v/v) of FBS and 1 % (v/v) of penicillin/streptomycin in a

humidified incubator (37 °C, 5 % CO_2). For this assay, MCF-7 cells and NHDF were seeded at a density of 1 x 10^4 cells/well in 96-well plates. After 24 h, the medium was removed, and cells were incubated with culture medium containing different doses of SBMA-BSA/GO for 24 or 48 h. Afterwards, the nanomaterials were removed, and the cells were incubated with 120 µL of fresh medium containing MTS (20 µL) for 4 h in the dark (37 °C, 5 % CO_2). Then, the cells' viability was determined by analyzing the absorbance of the samples at 490 nm, using a microplate reader (Bio-Rad xMark microplate spectrophotometer). Negative (K-) and positive (K+) controls correspond to cells incubated solely with culture medium (without nanomaterials) and to cells treated with ethanol (70 % (v/v)), respectively.

2.2.4. Evaluation of the phototherapeutic capacity of SBMA-BSA/GO and IR/SBMA-BSA/GO

The phototherapeutic effect mediated by SBMA-BSA/GO and IR/SBMA-BSA/GO was evaluated as previously described [38, 50]. In brief, MCF-7 cells were seeded as described in 2.2.3. After 24 h, the medium was replaced by fresh medium containing different concentrations of SBMA-BSA/GO (40.0 and 65.0 µg/mL of GO equivalents) or IR/SBMA-BSA/GO (40.0/7.7 and 65.0/12.5 µg/mL of GO/IR780 equivalents). After 4 h, cells were irradiated with NIR light (808 nm, 1.7 W/cm^2, 10 min). Upon 24 h of incubation, the nanoparticles were removed, and the cells' viability was evaluated as described in 2.2.3.

2.2.5. Statistical analysis

All data are presented as the mean ± Standard Deviation (S.D.). One-way Analysis of Variance (ANOVA) with the Student-Newman-Keuls test was applied for the comparison of multiple groups. A p value lower than 0.05 ($^*p < 0.05$) was considered statistically significant. For data analysis, GraphPad Prism v6.0 (Trial version, GraphPad Software, CA, USA) was used.

Chapter 3

Results and Discussion

3. Results and Discussion

3.1. Production and characterization of SBMA-BSA/GO and IR/SBMA-BSA/GO

For improving the colloidal stability and phototherapeutic capacity of GO, this nanomaterial was functionalized with SBMA-*g*-BSA and was loaded with IR780, respectively (Figure 6).

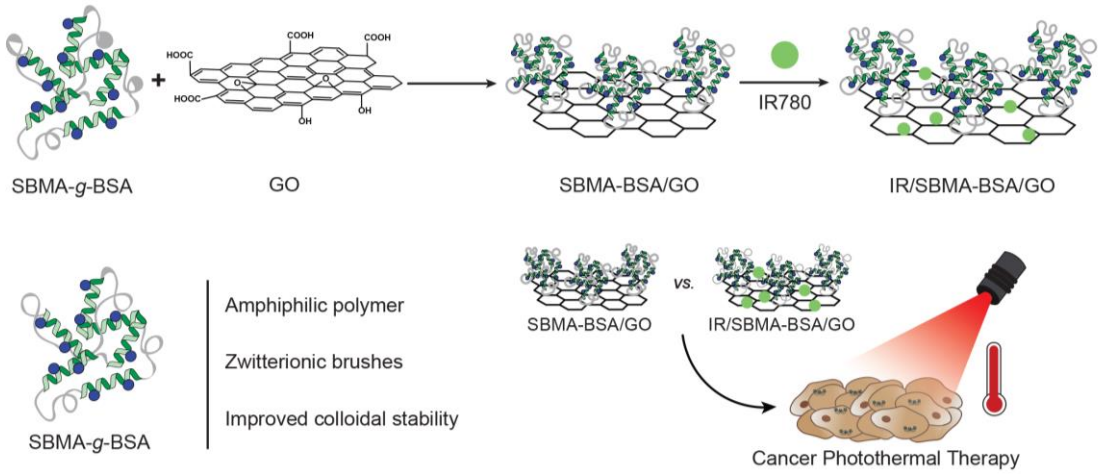

Figure 6: Schematic representation of the application of SBMA-BSA/GO and IR/SBMA-BSA/GO in cancer PTT.

The SBMA-*g*-BSA was synthesized as described by Alves *et al.* [88], by grafting SBMA into BSA using a Michael addition. The FTIR spectrum of SBMA showed its S=O stretch (at 1298 cm^{-1}) and C=O stretch (at 1715 cm^{-1}) characteristic peaks (Figure 7). Additionally, the spectrum of BSA showed peaks belonging to O-H (at 3284 cm^{-1}), C-H (at 2872 and 2958 cm^{-1}) and C=O (1644 cm^{-1}) vibrations. In the FTIR spectrum of SBMA-*g*-BSA, the characteristic peaks of the BSA functional groups are present as well as the S=O peak belonging to SBMA, hence confirming its successful synthesis.

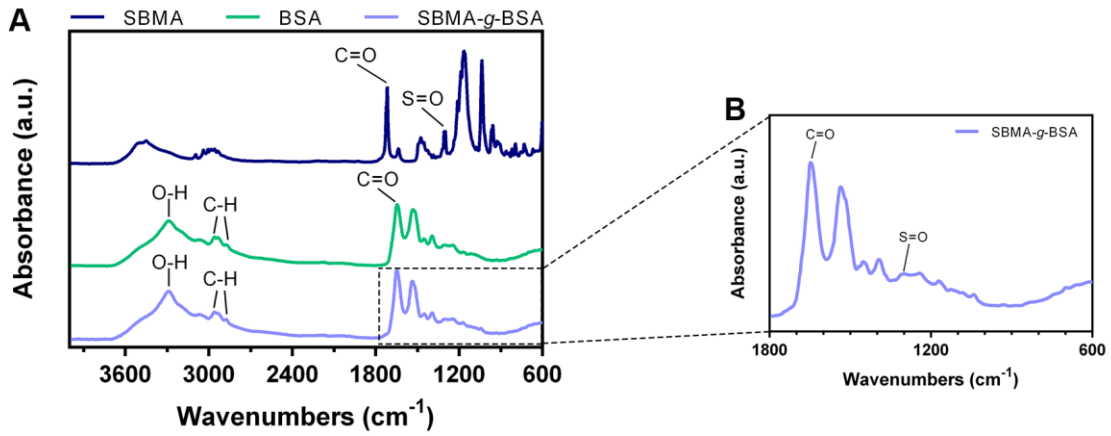

Figure 7: FTIR spectra of SBMA, BSA and SBMA-*g*-BSA (A). FTIR spectrum of SBMA-*g*-BSA in the 1800-600 cm^{-1} wavenumber range (B).

Then, GO was functionalized with SBMA-*g*-BSA by using a simple sonication process [50]. During this process, the hydrophobic domains of SBMA-*g*-BSA adsorb into GO aromatic surface, yielding SBMA-BSA/GO. The Dynamic Light Scattering (DLS) analysis demonstrated that the functionalization of GO with SBMA-*g*-BSA did not impact meaningfully on its size distribution (Figure 8). The nanosized dimensions of SBMA-BSA/GO were then confirmed by TEM (Figure 9), revealing that these are within the size distribution considered as optimal for passive tumor accumulation [32].

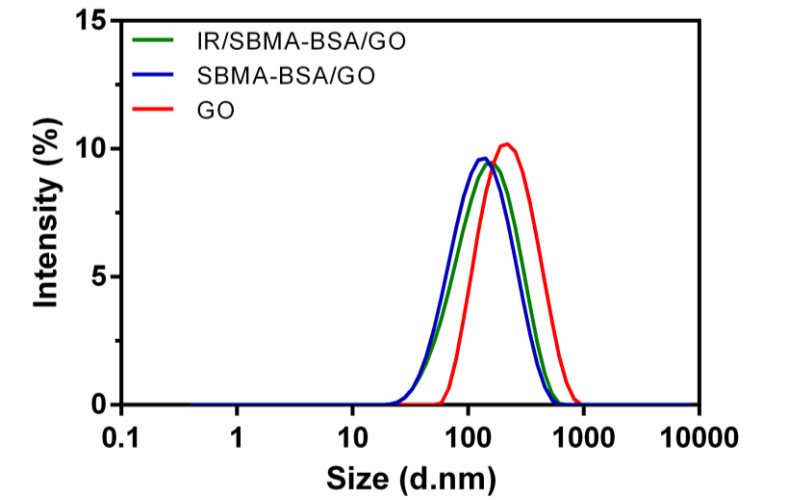

Figure 8: DLS size distribution of GO, SBMA-BSA/GO and IR/SBMA-BSA/GO.

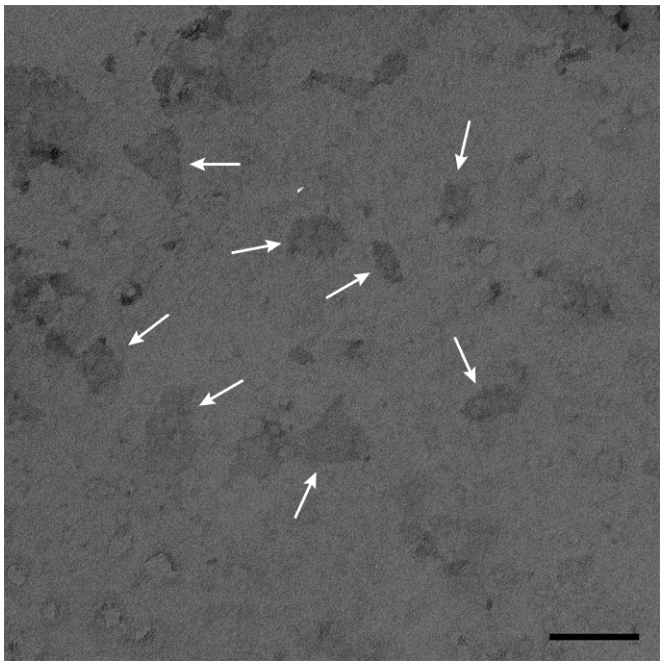

Figure 9: TEM analysis of SBMA-BSA/GO. The arrows indicate the nanomaterials. Scale bar corresponds to 200 nm.

Then, IR780 was loaded into the surface of SBMA-BSA/GO through non-covalent interactions (hydrophobic interactions and π-π stacking). The size distribution of IR/SBMA-BSA/GO was similar to that of SBMA-BSA/GO, indicating that the loading of this phototherapeutic agent does not impact significantly the nanomaterials' size (Figure 8). The zeta potential of SBMA-BSA/GO (−29.6 ± 0.9 mV) and IR/SBMA-BSA/GO (−29.4 ± 1.2 mV) were also comparable, indicating that both nanomaterials have an identical surface charge. In contrast, non-functionalized GO presented a more negative surface charge (−43.8 ± 1.3 mV), suggesting that the SBMA-*g*-BSA based coating can attenuate part of the negative surface charge displayed by the GO nanostructures. Moreover, the IR780 encapsulation efficiency in IR/SBMA-BSA/GO was of about 77 ± 14 %, which is higher than that displayed by other GO-based nanomaterials [97, 98]. Furthermore, the IR/SBMA-BSA/GO was capable of adsorbing 0.192 ± 0.043 μg of IR780 per μg of GO. This high drug loading capacity is an inherent property of GO based nanomaterials [38, 99], and also results from the fact that GO nanosheets without IR780 are removed during the nanomaterials' purification phase (centrifugation step).

Additionally, the stability of the SBMA-BSA/GO and IR/SBMA-BSA/GO overtime in cell culture medium (DMEM-F12 supplemented with 10 % (v/v) of FBS) was assessed (Figure 10). Both samples were capable of maintaining their size overtime (size variation < 8 % after 48 h of incubation), revealing an excellent colloidal stability. As control, the colloidal stability of GO coated with BSA (non-SBMA functionalized) was

also evaluated (Figure 10). In this regard, BSA/GO suffered an up to 31 % increase in its size when incubated in cell culture medium. These findings imply that the improved colloidal stability of SBMA-BSA/GO and IR/SBMA-BSA/GO results from the SBMA-functionalization. In fact, Alves *et al.* previously demonstrated that the grafting of SBMA into the surface of polymeric nanoparticles also enhances their colloidal stability [88]. Moreover, the coating of nanostructures with SBMA has been reported to decrease protein adsorption on the nanostructures' surface, hence increasing their stability during circulation and prompting their tumor accumulation [100-102]. Overall, the SBMA-BSA/GO and IR/SBMA-BSA/GO present suitable physicochemical properties for application in cancer therapy.

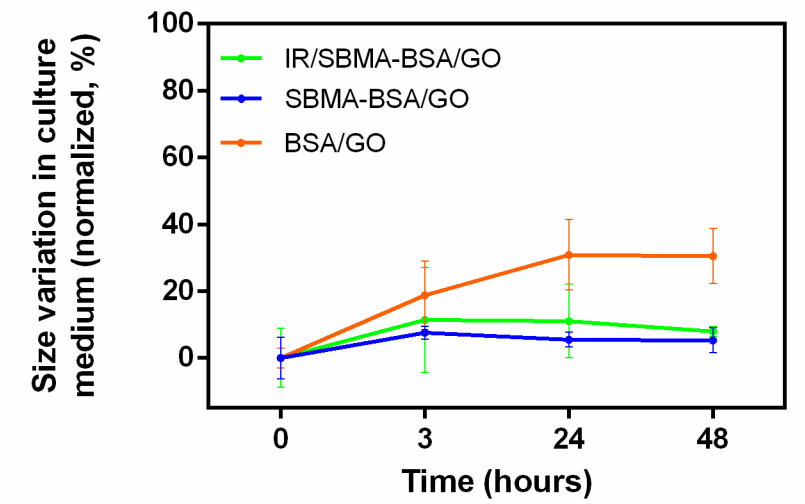

Figure 10: Size variation of BSA/GO, SBMA-BSA/GO and IR/SBMA-BSA/GO when dispersed in DMEM-F12 medium supplemented with 10 % of FBS (v/v). The values of each group were normalized using the respective initial size (t = 0 h). Each bar represents mean ± S.D. (n = 3).

3.2. Photothermal capacity of SBMA-BSA/GO and IR/SBMA-BSA/GO

To assess the ability of SBMA-BSA/GO and IR/SBMA-BSA/GO to interact with NIR light, their absorption spectra was acquired (Figure 11). As expected, SBMA-BSA/GO exhibited a NIR absorption as similar to that displayed by GO, confirming that the functionalization of GO with SBMA-*g*-BSA does not impair the nanosheets' ability to interact with NIR light (Figure 11). On the other hand, the spectrum of IR/SBMA-BSA/GO demonstrated an increased absorption in the 620-870 region, which is a characteristic feature of IR780 [88, 92, 103]. Due to this property, the IR/SBMA-BSA/GO presented a 5.6-times higher absorption at 808 nm than SBMA-BSA/GO (Figure 11). By taking into account that 808 nm laser light is going to

be used for irradiating the nanostructures, the enhanced absorption of IR/SBMA-BSA/GO at this wavelength is indicative of its higher photothermal potential.

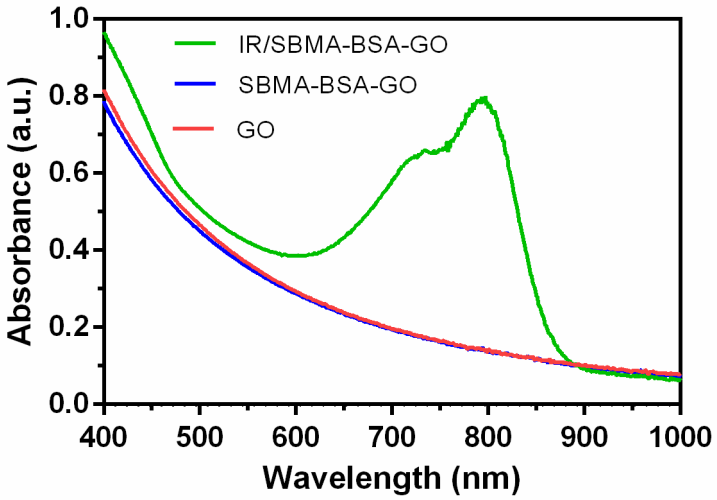

Figure 11: UV-Vis-NIR absorption spectra of GO, SBMA-BSA/GO and IR/SBMA-BSA/GO.

Then, the photothermal capacity of these nanomaterials was investigated (Figure 12). In general, SBMA-BSA/GO and IR/SBMA-BSA/GO produced a time- and concentration-dependent temperature increase when irradiated with NIR light (Figure 12A and 12B). After 10 min of irradiation, SBMA-BSA/GO and IR/SBMA-BSA/GO could generate a temperature increase of about 14 and 28 °C, respectively (at 65 µg/mL of GO equivalents) (Figure 12A and 12B). Reaching these temperature increases can potentially induce the death of cancer cells [27, 35]. Furthermore, the response of water (control) to NIR light irradiation was meaningless ($\Delta T < 2$ °C) (Figure 12A and 12B), which is justified by the weak interaction of 808 nm radiation with water [27].

The IR/SBMA-BSA/GO could produce an up to 2-times higher photoinduced heat than SBMA-BSA/GO. The higher photothermal capacity of IR/SBMA-BSA/GO is related to its higher NIR absorption (Figure 11). In this way, the incorporation of IR780 in SBMA-BSA/GO is a straightforward non-laborious process for improving the photothermal capacity of this nanomaterial. Furthermore, these results also suggest that the SBMA-functionalized GO nanomaterials may produce an on-demand therapeutic effect.

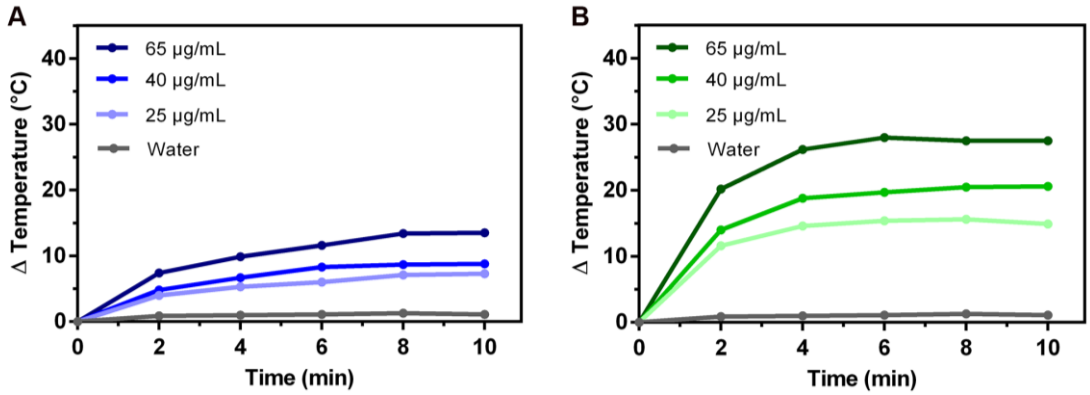

Figure 12: Characterization of the photothermal capacity of SBMA-BSA/GO and IR/SBMA-BSA/GO. Temperature variation curves of SBMA-BSA/GO (A) and IR/SBMA-BSA/GO (B) at different concentrations (of GO equivalents) during 10 min of NIR irradiation (808 nm, 1.7 W/cm^2).

Shi and co-workers reported that PEGylated GO-iron oxide-gold nanohybrids (10 mg/mL of GO equivalents) can generate a temperature increase of about 16 °C after NIR irradiation (808 nm, 1 W/cm^2, 5 min) [104]. Herein, the IR/SBMA-BSA/GO produced a temperature variation of 15 °C upon NIR laser irradiation (25 µg/mL of GO equivalents; 808 nm, 1.7 W/cm^2, 6 min), hence attesting its good photothermal capacity.

3.3. Evaluation of the cytocompatibility of SBMA-BSA/GO

Prior to determining the therapeutic capacity of the different SBMA-functionalized GO nanoformulations, the cytocompatibility of the SBMA-BSA/GO was investigated. For such, NHDF (healthy cell model) and MCF-7 cells (breast cancer cell model) were incubated with SBMA-BSA/GO during 24 and 48 h (Figure 13).

NHDF incubated with SBMA-BSA/GO did not have their viability affected in a meaningful way (cell viability > 92 %), even at a high SBMA-BSA/GO dose (75 µg/mL of GO equivalents) (Figure 13B). Furthermore, MCF-7 cells incubated with SBMA-BSA/GO also revealed a high cell viability (> 93 %) (Figure 13A). These results are in-line with the excellent cytocompatibility displayed by SBMA-functionalized nanomaterials and by BSA-based nanoformulations [89, 105-108]. Together, this data indicates the good cytocompatibility of SBMA-BSA/GO.

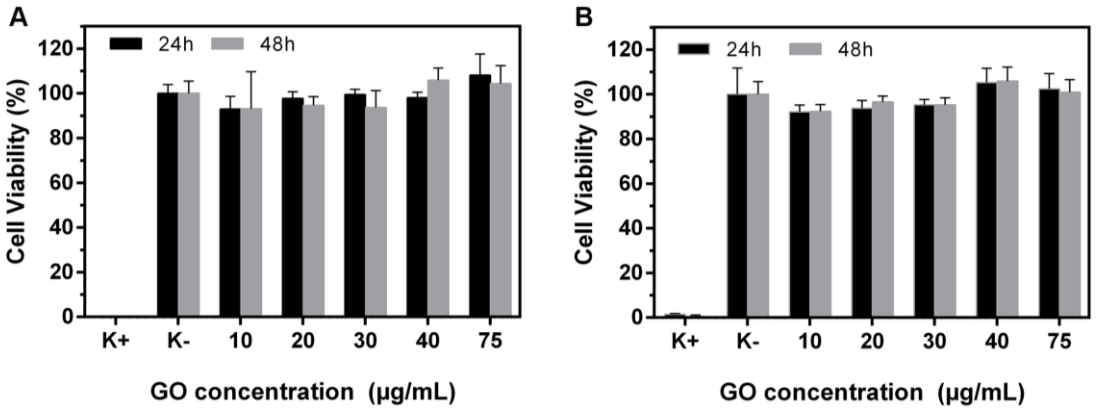

Figure 13: Evaluation of the cytocompatibility profile of SBMA-BSA/GO. Cell viability of MCF-7 cells (A) and NHDF (B) incubated with SBMA-BSA/GO at different concentrations (of GO equivalents) during 24 and 48 h. Data represent mean ± S.D., n = 5. K- and K+ represent negative and positive controls, respectively.

3.4. Evaluation of the photothermal therapy mediated by SBMA-BSA/GO and IR/SBMA-BSA/GO

Then, the phototherapeutic capacity of SBMA-BSA/GO and IR/SBMA-BSA/GO towards breast cancer cells was investigated. For this purpose, MCF-7 cells were incubated with the nanomaterials and then were exposed to NIR light (808 nm, 1.7 W/cm^2, 10 min) (Figure 14A).

As expected, MCF-7 cells solely incubated with SBMA-BSA/GO or only exposed to NIR light did not show a decrease in their viability (Figure 14B). Such result is in agreement with the good cytocompatibility displayed by SBMA-BSA/GO (Figure 13A) and with the insignificant off-target heating induced by water when exposed to NIR light (Figure 12). Surprisingly, the combination of NIR light with SBMA-BSA/GO did not reduce the viability of the cancer cells, even at a relatively high nanomaterial's dose (65 µg/mL of GO equivalents) - Figure 14B. This data further confirms the importance of improving GO photothermal capacity in order to achieve an appropriate therapeutic effect.

On the other hand, the two tested doses of non-irradiated IR/SBMA-BSA/GO (40.0/7.7 and 65.0/12.5 µg/mL of GO/IR780 equivalents) induced a similar reduction on cancer cells' viability to about 67 % (Figure 14B). This effect may result from the IR780 propensity to accumulate on the mitochondria of MCF-7 cells, leading to a slight cytotoxic effect [109, 110]. In turn, upon irradiation with NIR light, the IR/SBMA-BSA/GO could greatly decrease the viability of MCF-7 cells (Figure 14B). At the highest concentration tested (65.0/12.5 µg/mL of GO/IR780 equivalents), the combination of IR/SBMA-BSA/GO with NIR light caused the ablation of cancer cells (cell viability < 2 %) (Figure 14B). Considering that the interaction of SBMA-BSA/GO

with NIR light did not cause any cytotoxicity, this data confirms that the encapsulation of IR780 in the SBMA-functionalized GO can be pursued to improve its phototherapeutic capacity.

For instance, Sun *et al.* grew gold nanorods on the surface of GO materials, demonstrating that the photothermal therapy mediated by these hybrid structures could reduce cancer cells' viability to 17 % (808 nm, 0.8 W/cm^2, 10 min; 50 μg/mL of Au) [82]. On the other hand, Wu *et al.* performed the growth of CuS nanoparticles on the surface of GO nanosheets, verifying that this nanohybrid could induce a reduction of breast cancer cells' viability to 45 % upon NIR laser irradiation (940 nm, 4 W/cm^2, 5 min; 50 μg/mL of nanohybrids) [111]. Herein, IR/SBMA-BSA/GO were prepared by just encapsulating IR780 in SBMA-BSA/GO, rendering a hybrid nanosystem whose photothermal effect diminished cancer cells' viability to 2 % (808 nm, 1.7 W/cm^2, 10 min; 65.0/12.5 μg/mL of GO/IR780 equivalents). In this way, IR/SBMA-BSA/GO is a promising agent for application in the PTT of breast cancer cells.

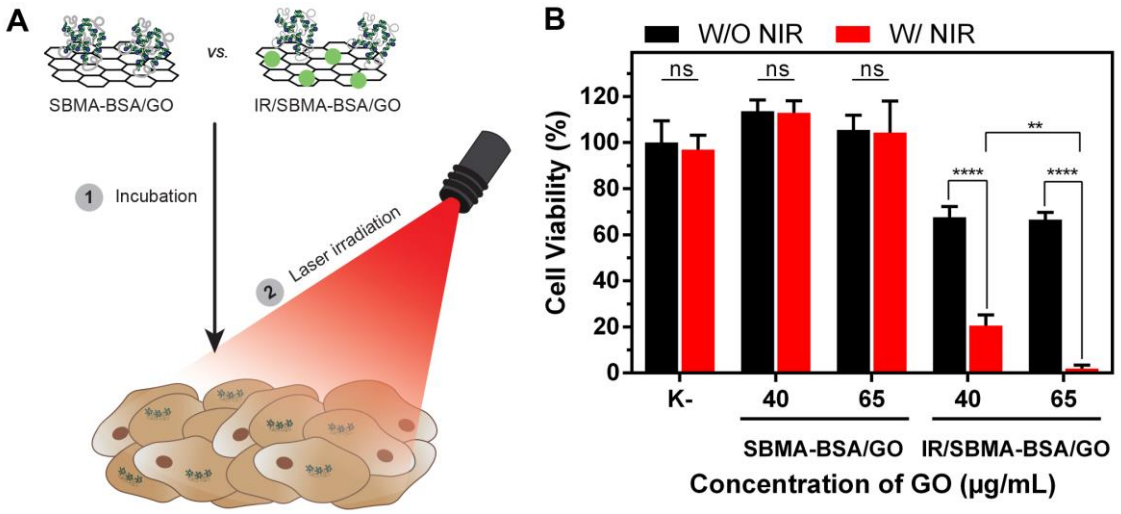

Figure 14: Evaluation of the phototherapeutic capacity of SBMA-BSA/GO and IR/SBMA-BSA/GO. Schematic representation of the PTT mediated by SBMA-BSA/GO and IR/SBMA-BSA/GO against MCF-7 cells (A). Phototherapeutic effect mediated by SBMA-BSA/GO and IR/SBMA-BSA/GO against MCF-7 cells without (W/O NIR) and with NIR (W/ NIR) laser irradiation (808 nm, 1.7 W/cm^2, 10 min) (B). K- W/O NIR represents the negative control. K- W/ NIR represents cells solely treated with NIR light. Data represents mean ± S.D., n = 5 (**$p < 0.01$; ****$p < 0.0001$), ns = non significant.

Chapter 4

Conclusion and Future Perspectives

4. Conclusion and Future Perspectives

Breast cancer remains as one of the main causes of death of women. The treatment of this disease relies on the use of chemo or radiotherapy, which not only have a sub-optimal therapeutic efficacy but also induce severe side effects on patients. This lack of efficacy and safety is a major contributor for the high mortality rates associated with this disease.

To overcome this situation, researchers have been developing new approaches to improve breast cancer treatment (*e.g.* immunotherapy, nanomaterial-based drug delivery). In particular, nanomaterials' mediated PTT has been receiving an increasing interest for cancer treatment. This therapeutic modality employs NIR-responsive nanomaterials that, due to their specific set of physicochemical characteristics, can accumulate within the tumor microenvironment. Then, upon NIR laser irradiation, these nanomaterials mediate a tumor-confined hyperthermia that can ablate the cancer cells.

The high NIR absorption displayed by GO as well as its ability to encapsulate a wide variety of therapeutics on its lattice render this nanomaterial a remarkable potential for cancer PTT. However, as-synthesized GO presents a poor colloidal stability (precipitating in biological fluids) and a subpar photothermal capacity (demanding the use of high doses/intense radiation), limiting its direct use in cancer PTT. Therefore, addressing these problems is of utmost importance for the future translation of GO-based PTT.

In the MSc research work performed, GO was functionalized with SBMA-*g*-BSA and was loaded with IR780, for the first time, in order to improve its colloidal stability and photothermal capacity. The SBMA-BSA/GO and IR/SBMA-BSA/GO were produced using a simple sonication method, and both of them presented an adequate size distribution. When in contact with biologically relevant media, the size of SBMA-BSA/GO and IR/SBMA-BSA/GO only increased by 8 % after 48 h, revealing an excellent colloidal stability. In the same condition, the BSA/GO suffered a 31 % increase in its size. By loading IR780 into SBMA-BSA/GO, the nanomaterials' NIR absorption increased by 5.6-fold. In this way, the IR/SBMA-BSA/GO could produce a up to 2-times higher photoinduced heat than SBMA-BSA/GO. In *in vitro* cell studies, the combination of NIR light with SBMA-BSA/GO did not induce photocytotoxicity on breast cancer cells. In stark contrast, the interaction of IR/SBMA-BSA/GO with NIR

light was able to induce the ablation of cancer cells (cell viability < 2 %). Overall, IR/SBMA-BSA/GO displays a greatly improved colloidal stability and phototherapeutic capacity, being a promising nanohybrid for application in the PTT of breast cancer cells.

In the near future, it will be interesting to investigate the phototherapeutic capacity of IR/SBMA-BSA/GO in spheroids. This 3D *in vitro* cancer model can mimic the key features presented by *in vivo* solid tumors (*e.g.* 3D architecture, microenvironment gradients, and biochemical/physical resistance patterns), hence giving important insights about the potential of this nanoformulation [112, 113]. Moreover, the IR/SBMA-BSA/GO can be coated with targeting ligand-polycation conjugates (*e.g.* folic acid-chitosan conjugate) through electrostatic interactions. Such may be a convenient route to incorporate targeting ligands on the IR/SBMA-BSA/GO, hence possibility improving the selectivity of this nanomaterial towards cancer cells. On the other hand, this approach opens the possibility for studying the optimal ligand density for a selective uptake by controlling the grafting degree of the ligand in the polymer backbone.

Chapter 5

Bibliographic References

5. Bibliographic References

[1] Siegel, R.L., K.D. Miller, and A. Jemal, *Cancer statistics, 2020*. CA: A Cancer Journal for Clinicians, (2020). 70(1): 7-30.

[2] Floor, S.L., J.E. Dumont, C. Maenhaut, and E. Raspe, *Hallmarks of cancer: of all cancer cells, all the time?* Trends in Molecular Medicine, (2012). 18(9): 509-515.

[3] Hanahan, D. and R.A. Weinberg, *Biological hallmarks of cancer*. Holland-Frei Cancer Medicine, (2016): 1-10.

[4] Hanahan, D. and Robert A. Weinberg, *Hallmarks of Cancer: The Next Generation*. Cell, (2011). 144(5): 646-674.

[5] Pietras, K. and A. Östman, *Hallmarks of cancer: Interactions with the tumor stroma*. Experimental Cell Research, (2010). 316(8): 1324-1331.

[6] Tiash, S. and E.H. Chowdhury, *Growth factor receptors: promising drug targets in cancer*. Journal of Cancer Metastasis and Treatment, (2015). 1: 190-200.

[7] Cavallaro, U. and G. Christofori, *Cell adhesion and signalling by cadherins and Ig-CAMs in cancer*. Nature Reviews Cancer, (2004). 4(2): 118-132.

[8] Hanahan, D. and R.A. Weinberg, *The hallmarks of cancer*. Cell, (2000). 100(1): 57-70.

[9] Masoud, G.N. and W. Li, *HIF-1α pathway: role, regulation and intervention for cancer therapy*. Acta Pharmaceutica Sinica B, (2015). 5(5): 378-389.

[10] Pugh, C.W. and P.J. Ratcliffe, *Regulation of angiogenesis by hypoxia: role of the HIF system*. Nature Medicine, (2003). 9(6): 677-684.

[11] Chen, X.-s., L.-y. Li, Y.-d. Guan, J.-m. Yang, and Y. Cheng, *Anticancer strategies based on the metabolic profile of tumor cells: therapeutic targeting of the Warburg effect*. Acta Pharmacologica Sinica, (2016). 37(8): 1013-1019.

[12] Fan, T., G. Sun, X. Sun, L. Zhao, R. Zhong, and Y. Peng, *Tumor energy metabolism and potential of 3-bromopyruvate as an inhibitor of aerobic glycolysis: Implications in tumor treatment*. Cancers, (2019). 11(3): 317.

[13] Vinay, D.S., E.P. Ryan, G. Pawelec, W.H. Talib, J. Stagg, E. Elkord, T. Lichtor, W.K. Decker, R.L. Whelan, H.M.C.S. Kumara, E. Signori, K. Honoki, A.G. Georgakilas, A. Amin, W.G. Helferich, C.S. Boosani, G. Guha, M.R. Ciriolo, S. Chen, S.I. Mohammed, A.S. Azmi, W.N. Keith, A. Bilsland, D. Bhakta, D. Halicka, H. Fujii, K. Aquilano, S.S. Ashraf, S. Nowsheen, X. Yang, B.K. Choi, and B.S. Kwon, *Immune evasion in cancer: Mechanistic basis and therapeutic strategies*. Seminars in Cancer Biology, (2015). 35: S185-S198.

[14] Mittal, D., M.M. Gubin, R.D. Schreiber, and M.J. Smyth, *New insights into cancer immunoediting and its three component phases—elimination, equilibrium and escape*. Current Opinion in Immunology, (2014). 27: 16-25.

[15] Yao, H., H. Wang, C. Li, J.-Y. Fang, and J. Xu, *Cancer Cell-Intrinsic PD-1 and Implications in Combinatorial Immunotherapy*. Frontiers in Immunology, (2018). 9(1774).

[16] Arasanz, H., M. Gato-Cañas, M. Zuazo, M. Ibañez-Vea, K. Breckpot, G. Kochan, and D. Escors, *PD1 signal transduction pathways in T cells*. Oncotarget, (2017). 8(31): 51936.

[17] Feng, Y., M. Spezia, S. Huang, C. Yuan, Z. Zeng, L. Zhang, X. Ji, W. Liu, B. Huang, W. Luo, B. Liu, Y. Lei, S. Du, A. Vuppalapati, H.H. Luu, R.C. Haydon, T.-C. He, and G. Ren, *Breast cancer development and progression: Risk factors, cancer stem cells, signaling pathways, genomics, and molecular pathogenesis*. Genes & Diseases, (2018). 5(2): 77-106.

[18] Cancro da mama. Accessed in: *https://www.ligacontracancro.pt/cancro-da-mama/*. Consulted in: 21/04/2020.

[19] Key, T.J., P.K. Verkasalo, and E. Banks, *Epidemiology of breast cancer*. The Lancet Oncology, (2001). 2(3): 133-140.

[20] Sopel, M., *The myoepithelial cell: its role in normal mammary glands and breast cancer*. Folia morphologica, (2010). 69(1): 1-14.

[21] Runa, F., S. Hamalian, K. Meade, P. Shisgal, P.C. Gray, and J.A. Kelber, *Tumor Microenvironment Heterogeneity: Challenges and Opportunities*. Current Molecular Biology Reports, (2017). 3(4): 218-229.

[22] Santi, A., F.G. Kugeratski, and S. Zanivan, *Cancer Associated Fibroblasts: The Architects of Stroma Remodeling*. PROTEOMICS, (2018). 18(5-6): 1700167.

[23] Place, A.E., S. Jin Huh, and K. Polyak, *The microenvironment in breast cancer progression: biology and implications for treatment*. Breast Cancer Research, (2011). 13(6): 227.

[24] Rebucci, M. and C. Michiels, *Molecular aspects of cancer cell resistance to chemotherapy*. Biochemical Pharmacology, (2013). 85(9): 1219-1226.

[25] Waks, A.G. and E.P. Winer, *Breast cancer treatment*. Jama, (2019). 321(3): 316-316.

[26] Wang, J., K. Lei, and F. Han, *Tumor microenvironment: recent advances in various cancer treatments*. European Review for Medical and Pharmacological Sciences, (2018). 22: 3855-3864.

[27] de Melo-Diogo, D., C. Pais-Silva, D.R. Dias, A.F. Moreira, and I.J. Correia, *Strategies to improve cancer photothermal therapy mediated by nanomaterials*. Advanced Healthcare Materials, (2017). 6(10): 1700073.

[28] Fernandes, N., C.F. Rodrigues, A.F. Moreira, and I.J. Correia, *Overview of the application of inorganic nanomaterials in cancer photothermal therapy*. Biomaterials Science, (2020).

[29] Liu, Y., P. Bhattarai, Z. Dai, and X. Chen, *Photothermal therapy and photoacoustic imaging via nanotheranostics in fighting cancer*. Chemical Society Reviews, (2019). 48(7): 2053-2108.

[30] Cheng, L., C. Wang, L. Feng, K. Yang, and Z. Liu, *Functional Nanomaterials for Phototherapies of Cancer*. Chemical Reviews, (2014). 114(21): 10869-10939.

[31] Wilhelm, S., A.J. Tavares, Q. Dai, S. Ohta, J. Audet, H.F. Dvorak, and W.C.W. Chan, *Analysis of nanoparticle delivery to tumours*. Nature Reviews Materials, (2016). 1(5): 16014.

[32] Blanco, E., H. Shen, and M. Ferrari, *Principles of nanoparticle design for overcoming biological barriers to drug delivery*. Nature Biotechnology, (2015). 33(9): 941-951.

[33] Danhier, F., *To exploit the tumor microenvironment: Since the EPR effect fails in the clinic, what is the future of nanomedicine?* Journal of Controlled Release, (2016). 244: 108-121.

[34] Matsumoto, Y., J.W. Nichols, K. Toh, T. Nomoto, H. Cabral, Y. Miura, R.J. Christie, N. Yamada, T. Ogura, M.R. Kano, Y. Matsumura, N. Nishiyama, T. Yamasoba, Y.H. Bae, and K. Kataoka, *Vascular bursts enhance permeability of tumour blood vessels and improve nanoparticle delivery*. Nature Nanotechnology, (2016). 11(6): 533-538.

[35] Chu, K.F. and D.E. Dupuy, *Thermal ablation of tumours: biological mechanisms and advances in therapy*. Nature Reviews Cancer, (2014). 14(3): 199-208.

[36] Bavli, Y., I. Winkler, B.M. Chen, S. Roffler, R. Cohen, J. Szebeni, and Y. Barenholz, *Doxebo (doxorubicin-free Doxil-like liposomes) is safe to use as a pre-treatment to prevent infusion reactions to PEGylated nanodrugs*. Journal of Controlled Release, (2019). 306: 138-148.

[37] Suk, J.S., Q. Xu, N. Kim, J. Hanes, and L.M. Ensign, *PEGylation as a strategy for improving nanoparticle-based drug and gene delivery*. Advanced Drug Delivery Reviews, (2016). 99: 28-51.

[38] de Melo-Diogo, D., E.C. Costa, C.G. Alves, R. Lima-Sousa, P. Ferreira, R.O. Louro, and I.J. Correia, *POxylated graphene oxide nanomaterials for combination chemo-phototherapy of breast cancer cells*. European Journal of Pharmaceutics and Biopharmaceutics, (2018). 131: 162-169.

[39] Hou, L., J. Fang, W. Wang, Z. Xie, D. Dong, and N. Zhang, *Indocyanine green-functionalized bottle brushes of poly (2-oxazoline) on cellulose nanocrystals for photothermal cancer therapy*. Journal of Materials Chemistry B, (2017). 5(18): 3348-3354.

[40] Yuan, Y.Y., C.Q. Mao, X.J. Du, J.Z. Du, F. Wang, and J. Wang, *Surface charge switchable nanoparticles based on zwitterionic polymer for enhanced drug delivery to tumor*. Advanced Materials, (2012). 24(40): 5476-5480.

[41] Ou, H., T. Cheng, Y. Zhang, J. Liu, Y. Ding, J. Zhen, W. Shen, Y. Xu, W. Yang, P. Niu, J. Liu, Y. An, Y. Liu, and L. Shi, *Surface-adaptive zwitterionic nanoparticles for prolonged blood circulation time and enhanced cellular uptake in tumor cells*. Acta Biomaterialia, (2018). 65: 339-348.

[42] Pelegri-O'Day, E.M., E.-W. Lin, and H.D. Maynard, *Therapeutic protein–polymer conjugates: advancing beyond PEGylation*. Journal of the American Chemical Society, (2014). 136(41): 14323-14332.

[43] Zhang, Y., Y. Liu, B. Ren, D. Zhang, S. Xie, Y. Chang, J. Yang, J. Wu, L. Xu, and J. Zheng, *Fundamentals and applications of zwitterionic antifouling polymers*. Journal of Physics D: Applied Physics, (2019). 52(40): 403001.

[44] Narmani, A., M. Rezvani, B. Farhood, P. Darkhor, J. Mohammadnejad, B. Amini, S. Refahi, and N. Abdi Goushbolagh, *Folic acid functionalized nanoparticles as pharmaceutical carriers in drug delivery systems*. Drug Development Research, (2019). 80(4): 404-424.

[45] Riaz, M.K., M.A. Riaz, X. Zhang, C. Lin, K.H. Wong, X. Chen, G. Zhang, A. Lu, and Z. Yang, *Surface functionalization and targeting strategies of liposomes in solid tumor therapy: A review*. Internationa Journal of Molecular Sciences, (2018). 19(1): 195.

[46] Mattheolabakis, G., L. Milane, A. Singh, and M.M. Amiji, *Hyaluronic acid targeting of CD44 for cancer therapy: from receptor biology to nanomedicine*. Journal of Drug Targeting, (2015). 23(7-8): 605-618.

[47] Yang, K., H. Xu, L. Cheng, C. Sun, J. Wang, and Z. Liu, *In vitro and in vivo near-infrared photothermal therapy of cancer using polypyrrole organic nanoparticles*. Advanced Materials, (2012). 24(41): 5586-5592.

[48] Jacinto, T.A., C.F. Rodrigues, A.F. Moreira, S.P. Miguel, E.C. Costa, P. Ferreira, and I.J. Correia, *Hyaluronic acid and vitamin E polyethylene glycol succinate functionalized gold-core silica shell nanorods for cancer targeted photothermal therapy*. Colloids and Surfaces B: Biointerfaces, (2020). 188: 110778.

[49] Sun, Q., J. Wu, L. Jin, L. Hong, F. Wang, Z. Mao, and M. Wu, *Cancer cell membrane-coated gold nanorods for photothermal therapy and radiotherapy on oral squamous cancer*. Journal of Materials Chemistry B, (2020).

[50] Lima-Sousa, R., D. de Melo-Diogo, C.G. Alves, E.C. Costa, P. Ferreira, R.O. Louro, and I.J. Correia, *Hyaluronic acid functionalized green reduced graphene oxide for targeted cancer photothermal therapy*. Carbohydrate Polymers, (2018). 200: 93-99.

[51] Jun, S.W., P. Manivasagan, J. Kwon, V.T. Nguyen, S. Mondal, C.D. Ly, J. Lee, Y.-H. Kang, C.-S. Kim, and J. Oh, *Folic acid–conjugated chitosan-functionalized graphene oxide for highly efficient photoacoustic imaging-guided tumor-targeted photothermal therapy*. International Journal of Biological Macromolecules, (2020). 155: 961-971.

[52] Yoon, H.-J., H.-S. Lee, J.-Y. Lim, and J.-H. Park, *Liposomal Indocyanine Green for Enhanced Photothermal Therapy*. ACS Applied Materials & Interfaces, (2017). 9(7): 5683-5691.

[53] Hu, D., J. Zhang, G. Gao, Z. Sheng, H. Cui, and L. Cai, *Indocyanine green-loaded polydopamine-reduced graphene oxide nanocomposites with amplifying photoacoustic and photothermal effects for cancer theranostics*. Theranostics, (2016). 6(7): 1043.

[54] Xu, J., A. Gulzar, Y. Liu, H. Bi, S. Gai, B. Liu, D. Yang, F. He, and P. Yang, *Integration of IR-808 sensitized upconversion nanostructure and MoS2 nanosheet for 808 nm NIR light triggered phototherapy and bioimaging*. Small, (2017). 13(36): 1701841.

[55] Luo, S., Z. Yang, X. Tan, Y. Wang, Y. Zeng, Y. Wang, C. Li, R. Li, and C. Shi, *Multifunctional photosensitizer grafted on polyethylene glycol and polyethylenimine dual-functionalized nanographene oxide for cancer-targeted near-infrared imaging and synergistic phototherapy*. ACS Applied Materials & Interfaces, (2016). 8(27): 17176-17186.

[56] Yang, K., J. Wan, S. Zhang, B. Tian, Y. Zhang, and Z. Liu, *The influence of surface chemistry and size of nanoscale graphene oxide on photothermal therapy of cancer using ultra-low laser power*. Biomaterials, (2012). 33(7): 2206-2214.

[57] Sahu, A., W.I. Choi, J.H. Lee, and G. Tae, *Graphene oxide mediated delivery of methylene blue for combined photodynamic and photothermal therapy*. Biomaterials, (2013). 34(26): 6239-6248.

[58] de Melo-Diogo, D., R. Lima-Sousa, C.G. Alves, E.C. Costa, R.O. Louro, and I.J. Correia, *Functionalization of graphene family nanomaterials for application in cancer therapy*. Colloids and Surfaces B: Biointerfaces, (2018). 171: 260-275.

[59] Singh, D.P., C.E. Herrera, B. Singh, S. Singh, R.K. Singh, and R. Kumar, *Graphene oxide: An efficient material and recent approach for biotechnological and biomedical applications*. Materials Science and Engineering: C, (2018). 86: 173-197.

[60] Priyadarsini, S., S. Mohanty, S. Mukherjee, S. Basu, and M. Mishra, *Graphene and graphene oxide as nanomaterials for medicine and biology application*. Journal of Nanostructure in Chemistry, (2018). 8(2): 123-137.

[61] Marcano, D.C., D.V. Kosynkin, J.M. Berlin, A. Sinitskii, Z. Sun, A. Slesarev, L.B. Alemany, W. Lu, and J.M. Tour, *Improved Synthesis of Graphene Oxide*. ACS Nano, (2010). 4(8): 4806-4814.

[62] Gonçalves, G., M. Vila, M.T. Portolés, M. Vallet-Regi, J. Gracio, and P.A.A. Marques, *Nano-graphene oxide: a potential multifunctional platform for cancer therapy*. Advanced Healthcare Materials, (2013). 2(8): 1072-1090.

[63] Hou, P.-X., C. Liu, and H.-M. Cheng, *Purification of carbon nanotubes*. Carbon, (2008). 46(15): 2003-2025.

[64] Scaletti, F., C.S. Kim, L. Messori, and V.M. Rotello, *Rapid purification of gold nanorods for biomedical applications*. MethodsX, (2014). 1: 118-123.

[65] de Melo-Diogo, D., R. Lima-Sousa, C.G. Alves, and I.J. Correia, *Graphene family nanomaterials for application in cancer combination photothermal therapy*. Biomaterials Science, (2019). 7(9): 3534-3551.

[66] Kiew, S.F., L.V. Kiew, H.B. Lee, T. Imae, and L.Y. Chung, *Assessing biocompatibility of graphene oxide-based nanocarriers: A review*. Journal of Controlled Release, (2016). 226: 217-228.

[67] Makharza, S., G. Cirillo, A. Bachmatiuk, I. Ibrahim, N. Ioannides, B. Trzebicka, S. Hampel, and M.H. Rümmeli, *Graphene oxide-based drug delivery vehicles: functionalization, characterization, and cytotoxicity evaluation*. Journal of Nanoparticle Research, (2013). 15(12): 2099.

[68] Liu, J., L. Cui, and D. Losic, *Graphene and graphene oxide as new nanocarriers for drug delivery applications*. Acta Biomaterialia, (2013). 9(12): 9243-9257.

[69] Hutanu, D., M.D. Frishberg, L. Guo, and C.C. Darie, *Recent applications of polyethylene glycols (PEGs) and PEG derivatives*. Modern Chemistry & Applications, (2014). 2(2): 1-6.

[70] Jokerst, J.V., T. Lobovkina, R.N. Zare, and S.S. Gambhir, *Nanoparticle PEGylation for imaging and therapy*. Nanomedicine, (2011). 6(4): 715-728.

[71] Parveen, S. and S.K. Sahoo, *Long circulating chitosan/PEG blended PLGA nanoparticle for tumor drug delivery*. European Journal of Pharmacology, (2011). 670(2): 372-383.

[72] Yang, K., S. Zhang, G. Zhang, X. Sun, S.-T. Lee, and Z. Liu, *Graphene in mice: ultrahigh in vivo tumor uptake and efficient photothermal therapy*. Nano Letters, (2010). 10(9): 3318-3323.

[73] Luo, N., J.K. Weber, S. Wang, B. Luan, H. Yue, X. Xi, J. Du, Z. Yang, W. Wei, R. Zhou, and G. Ma, *PEGylated graphene oxide elicits strong immunological responses despite surface passivation*. Nature Communications, (2017). 8(1): 14537.

[74] Hoang Thi, T.T., E.H. Pilkington, D.H. Nguyen, J.S. Lee, K.D. Park, and N.P. Truong, *The Importance of Poly (ethylene glycol) Alternatives for Overcoming PEG Immunogenicity in Drug Delivery and Bioconjugation*. Polymers, (2020). 12(2): 298.

[75] Mohamed, M., A.S. Abu Lila, T. Shimizu, E. Alaaeldin, A. Hussein, H.A. Sarhan, J. Szebeni, and T. Ishida, *PEGylated liposomes: immunological responses*. Science and Technology of Advanced Materials, (2019). 20(1): 710-724.

[76] Yin, T., J. Liu, Z. Zhao, Y. Zhao, L. Dong, M. Yang, J. Zhou, and M. Huo, *Redox sensitive hyaluronic acid-decorated graphene oxide for photothermally controlled tumor-cytoplasm-selective rapid drug delivery*. Advanced Functional Materials, (2017). 27(14): 1604620.

[77] Pei, S. and H.-M. Cheng, *The reduction of graphene oxide*. Carbon, (2012). 50(9): 3210-3228.

[78] Gao, X., J. Jang, and S. Nagase, *Hydrazine and Thermal Reduction of Graphene Oxide: Reaction Mechanisms, Product Structures, and Reaction Design*. The Journal of Physical Chemistry C, (2010). 114(2): 832-842.

[79] Robinson, J.T., S.M. Tabakman, Y. Liang, H. Wang, H. Sanchez Casalongue, D. Vinh, and H. Dai, *Ultrasmall reduced graphene oxide with high near-infrared absorbance for photothermal therapy*. Journal of the American Chemical Society, (2011). 133(17): 6825-6831.

[80] Qi, Y., T. Xia, Y. Li, L. Duan, and W. Chen, *Colloidal stability of reduced graphene oxide materials prepared using different reducing agents*. Environmental Science: Nano, (2016). 3(5): 1062-1071.

[81] Bullock, C.J. and C. Bussy, *Biocompatibility considerations in the design of graphene biomedical materials*. Advanced Materials Interfaces, (2019). 6(11): 1900229.

[82] Sun, B., J. Wu, S. Cui, H. Zhu, W. An, Q. Fu, C. Shao, A. Yao, B. Chen, and D. Shi, *In situ synthesis of graphene oxide/gold nanorods theranostic hybrids for efficient tumor computed tomography imaging and photothermal therapy*. Nano Research, (2017). 10(1): 37-48.

[83] Xu, C., D. Yang, L. Mei, Q. Li, H. Zhu, and T. Wang, *Targeting chemophotothermal therapy of hepatoma by gold nanorods/graphene oxide core/shell nanocomposites*. ACS Applied Materials & Interfaces, (2013). 5(24): 12911-12920.

[84] Sun, H., M.Y.Z. Chang, W.-I. Cheng, Q. Wang, A. Commisso, M. Capeling, Y. Wu, and C. Cheng, *Biodegradable zwitterionic sulfobetaine polymer and its conjugate with paclitaxel for sustained drug delivery*. Acta Biomaterialia, (2017). 64: 290-300.

[85] Wu, J., W. Lin, Z. Wang, S. Chen, and Y. Chang, *Investigation of the hydration of nonfouling material poly (sulfobetaine methacrylate) by low-field nuclear magnetic resonance*. Langmuir, (2012). 28(19): 7436-7441.

[86] Yu, J., Y. Liu, S. Song, G. Gao, and F. Liu, *Phase behavior of a high-concentration sulfobetaine zwitterionic polymer solution*. Polymer Journal, (2017). 49(11): 767-774.

[87] Ladd, J., Z. Zhang, S. Chen, J.C. Hower, and S. Jiang, *Zwitterionic polymers exhibiting high resistance to nonspecific protein adsorption from human serum and plasma*. Biomacromolecules, (2008). 9(5): 1357-1361.

[88] Alves, C.G., D. de Melo-Diogo, R. Lima-Sousa, and I.J. Correia, *IR780 loaded sulfobetaine methacrylate-functionalized albumin nanoparticles aimed for enhanced breast cancer phototherapy*. International Journal of Pharmaceutics, (2020). 582: 119346.

[89] Almutary, A.G., B.J. Sanderson, Z. Alhalili, and A.V. Ellis, *Toxicity of thiolated silica nanoparticles modified with sulfobetaine methacrylate for potential use in chemotherapy drug conjugation*. Journal of Applied Pharmaceutical Science, (2017). 7(07): 001-009.

[90] Men, Y., S. Peng, P. Yang, Q. Jiang, Y. Zhang, B. Shen, P. Dong, Z. Pang, and W. Yang, *Biodegradable Zwitterionic Nanogels with Long Circulation for Antitumor Drug Delivery*. ACS Applied Materials & Interfaces, (2018). 10(28): 23509-23521.

[91] Nagy-Simon, T., M. Potara, A.M. Craciun, E. Licarete, and S. Astilean, *IR780-dye loaded gold nanoparticles as new near infrared activatable nanotheranostic agents for simultaneous photodynamic and photothermal therapy and intracellular tracking by surface enhanced resonant Raman scattering imaging*. Journal of Colloid and Interface Science, (2018). 517: 239-250.

[92] Alves, C.G., R. Lima-Sousa, D. de Melo-Diogo, R.O. Louro, and I.J. Correia, *IR780 based nanomaterials for cancer imaging and photothermal, photodynamic and combinatorial therapies*. International Journal of Pharmaceutics, (2018). 542(1): 164-175.

[93] Leitão, M.M., D. de Melo-Diogo, C.G. Alves, R. Lima-Sousa, and I.J. Correia, *Prototypic Heptamethine Cyanine Incorporating Nanomaterials for Cancer Phototheragnostic*. Advanced Healthcare Materials, (2020). 9(6): 1901665.

[94] Zhang, H., Z. Zhu, Y. Wang, Z. Fei, and J. Cao, *Changing the activities and structures of bovine serum albumin bound to graphene oxide*. Applied Surface Science, (2018). 427: 1019-1029.

[95] de Melo-Diogo, D., C. Pais-Silva, E.C. Costa, R.O. Louro, and I.J. Correia, *D-α-tocopheryl polyethylene glycol 1000 succinate functionalized nanographene oxide for cancer therapy*. Nanomedicine, (2017). 12(5): 443-456.

[96] Cabral, C.S.D., S.P. Miguel, D. de Melo-Diogo, R.O. Louro, and I.J. Correia, *Green reduced graphene oxide functionalized 3D printed scaffolds for bone tissue regeneration*. Carbon, (2019). 146: 513-523.

[97] Mahajan, C.R., L.B. Joshi, U. Varma, J.B. Naik, V.R. Chaudhari, and S. Mishra, *Sustainable Drug Delivery of Famotidine Using Chitosan-Functionalized Graphene Oxide as Nanocarrier*. Global Challenges, (2019). 3(10): 1900002.

[98] Chauhan, D.S., M.K. Kumawat, R. Prasad, P.K. Reddy, M. Dhanka, S.K. Mishra, R. Bahadur, S. Neekhra, A. De, and R. Srivastava, *Plasmonic carbon nanohybrids for repetitive and highly localized photothermal cancer therapy*. Colloids and Surfaces B: Biointerfaces, (2018). 172: 430-439.

[99] Yang, X., Y. Wang, X. Huang, Y. Ma, Y. Huang, R. Yang, H. Duan, and Y. Chen, *Multi-functionalized graphene oxide based anticancer drug-carrier with dual-targeting function and pH-sensitivity*. Journal of materials chemistry, (2011). 21(10): 3448-3454.

[100] Wu, J., C. He, H. He, C. Cheng, J. Zhu, Z. Xiao, H. Zhang, X. Li, J. Zheng, and J. Xiao, *Importance of zwitterionic incorporation into polymethacrylate-based hydrogels for simultaneously improving optical transparency, oxygen permeability, and antifouling properties*. Journal of Materials Chemistry B, (2017). 5(24): 4595-4606.

[101] Chang, Y., S. Chen, Z. Zhang, and S. Jiang, *Highly protein-resistant coatings from well-defined diblock copolymers containing sulfobetaines*. Langmuir, (2006). 22(5): 2222-2226.

[102] Peng, S., B. Ouyang, Y. Men, Y. Du, Y. Cao, R. Xie, Z. Pang, S. Shen, and W. Yang, *Biodegradable zwitterionic polymer membrane coating endowing nanoparticles with ultra-long circulation and enhanced tumor photothermal therapy*. Biomaterials, (2020). 231: 119680.

[103] Pais-Silva, C., D. de Melo-Diogo, and I.J. Correia, *IR780-loaded TPGS-TOS micelles for breast cancer photodynamic therapy*. European Journal of Pharmaceutics and Biopharmaceutics, (2017). 113: 108-117.

[104] Shi, X., H. Gong, Y. Li, C. Wang, L. Cheng, and Z. Liu, *Graphene-based magnetic plasmonic nanocomposite for dual bioimaging and photothermal therapy*. Biomaterials, (2013). 34(20): 4786-4793.

[105] Zhang, M., W. Shen, Q. Xiong, H. Wang, Z. Zhou, W. Chen, and Q. Zhang, *Thermo-responsiveness and biocompatibility of star-shaped poly [2-(dimethylamino) ethyl methacrylate]-b-poly (sulfobetaine methacrylate) grafted on a β-cyclodextrin core*. RSC Advances, (2015). 5(36): 28133-28140.

[106] Lin, T., P. Zhao, Y. Jiang, Y. Tang, H. Jin, Z. Pan, H. He, V.C. Yang, and Y. Huang, *Blood–Brain-Barrier-Penetrating Albumin Nanoparticles for Biomimetic Drug Delivery via Albumin-Binding Protein Pathways for Antiglioma Therapy*. ACS Nano, (2016). 10(11): 9999-10012.

[107] Dong, Y., R. Fu, J. Yang, P. Ma, L. Liang, Y. Mi, and D. Fan, *Folic acid-modified ginsenoside Rg5-loaded bovine serum albumin nanoparticles for targeted cancer therapy in vitro and in vivo*. International journal of nanomedicine, (2019). 14: 6971-6988.

[108] Yang, Z., N. Zhang, T. Ma, L. Liu, L. Zhao, and H. Xie, *Engineered bovine serum albumin-based nanoparticles with pH-sensitivity for doxorubicin delivery and controlled release*. Drug Delivery, (2020). 27(1): 1156-1164.

[109] Wang, Y., T. Liu, E. Zhang, S. Luo, X. Tan, and C. Shi, *Preferential accumulation of the near infrared heptamethine dye IR-780 in the mitochondria of drug-resistant lung cancer cells*. Biomaterials, (2014). 35(13): 4116-4124.

[110] Zhang, C., T. Liu, Y. Su, S. Luo, Y. Zhu, X. Tan, S. Fan, L. Zhang, Y. Zhou, and T. Cheng, *A near-infrared fluorescent heptamethine indocyanine dye with preferential tumor accumulation for in vivo imaging*. Biomaterials, (2010). 31(25): 6612-6617.

[111] Wu, C., A. Zhu, D. Li, L. Wang, H. Yang, H. Zeng, and Y. Liu, *Photosensitizer-assembled PEGylated graphene-copper sulfide nanohybrids as a synergistic near-infrared phototherapeutic agent*. Expert opinion on drug delivery, (2016). 13(1): 155-165.

[112] Nunes, A.S., A.S. Barros, E.C. Costa, A.F. Moreira, and I.J. Correia, *3D tumor spheroids as in vitro models to mimic in vivo human solid tumors resistance to therapeutic drugs*. Biotechnology and Bioengineering, (2019). 116(1): 206-226.

[113] Costa, E.C., A.F. Moreira, D. de Melo-Diogo, V.M. Gaspar, M.P. Carvalho, and I.J. Correia, *3D tumor spheroids: an overview on the tools and techniques used for their analysis*. Biotechnology Advances, (2016). 34(8): 1427-1441.